axioms

MDPI

Article

Mathematical Modeling and Forecasting of COVID-19 in Saudi Arabia under Fractal-Fractional Derivative in Caputo Sense with Power-Law

Mdi Begum Jeelani [1,*,†], Abeer S. Alnahdi [1,†], Mohammed S. Abdo [2,†], Mansour A. Abdulwasaa [3,†], Kamal Shah [4,†] and Hanan A. Wahash [5,†]

[1] Department of Mathematics, Imam Mohammad Ibn Saud Islamic University, Riyadh 11564, Saudi Arabia; asalnahdi@imamu.edu.sa
[2] Department of Mathematics, Hodeidah University, Al-Hodeidah 3114, Yemen; msabdo1977@gmail.com
[3] Department of Statistics, Dr. Babasaheb Ambedkar Marathwada University, Aurangabad 431004, India; mansalahdall37@yahoo.com
[4] Department of Mathematics, University of Malakand, Chakdara 18800, Pakistan; kamalshah408@gmail.com
[5] Department of Mathematics, Dr. Babasaheb Ambedkar Marathwada University, Aurangabad 431004, India; hawahash86@gmail.com
* Correspondence: mbshaikh@imamu.edu.sa
† These authors contributed equally to this work.

Abstract: This manuscript is devoted to investigating a fractional-order mathematical model of COVID-19. The corresponding derivative is taken in Caputo sense with power-law of fractional order μ and fractal dimension χ. We give some detailed analysis on the existence and uniqueness of the solution to the proposed problem. Furthermore, some results regarding basic reproduction number and stability are given. For the proposed theoretical analysis, we use fixed point theory while for numerical analysis fractional Adams–Bashforth iterative techniques are utilized. Using our numerical scheme is verified by using some real values of the parameters to plot the approximate solution to the considered model. Graphical presentations corresponding to different values of fractional order and fractal dimensions are given. Moreover, we provide some information regarding the real data of Saudi Arabia from 1 March 2020 till 22 April 2021, then calculated the fatality rates by utilizing the SPSS, Eviews and Expert Modeler procedure. We also built forecasts of infection for the period 23 April 2021 to 30 May 2021, with 95% confidence.

Keywords: Adams–Bashforth method; COVID-19; forecasting; fractal-fractional derivative; fixed point approach; SPSS program and expert modeler procedure; Matlab 16

Citation: Jeelani, B.M.; Alnahdi, A.S.; Abdo, M.S.; Abdulwasa, M.A.; Shah, K.; Wahash, H.A. Mathematical Modeling and Forecasting of COVID-19 in Saudi Arabia under Fractal-Fractional Derivative in Caputo Sense with Power-Law. *Axioms* **2021**, *10*, 228. https://doi.org/10.3390/axioms10030228

Academic Editor: Tatiana Odzijewicz

Received: 29 July 2021
Accepted: 6 September 2021
Published: 15 September 2021

1. Introduction

Recently the COVID-19 pandemic has greatly affected the whole world. The mentioned disease was originated in the end of 2019 in Wuhan city of China. Later on, the infection was transmitted throughout the whole globe in the next few months. WHO announced that it was a pandemic in the whole world. According to the reports published by WHO, nearly fifty million people have gotten infected around the globe in which more than three million people died. Many countries have implemented strict lockdown in their community advised the public to keep social distance. These necessary measures have produced some positive impact on the control of COVID-19 in various countries. The concerned infection has greatly destroyed the economical situation of various countries. Here we remark that some countries have now succeeded in creating COVID-19 vaccines including USA, UK, Germany, China, etc.

This disease spreads rapidly making it one of the most infectious and contagious diseases in today's world. Dry cough, fever, nausea, aches and pains, headache, breathlessness, fatigue, etc. are basic symptoms of COVID-19 patients. Among them, serious

symptoms include chest pain, high blood pressure, paralysis, and breathing difficulties. This disease takes 5–6 days to show the initial symptoms and can take up to 14 days to vanish or spread rapidly in the body of the infected person [1,2]. The infected person transfers this disease mostly by getting in contact with a normal person in any form such as by shaking hands, using the same utensils, or getting in contact with the saliva droplets of the infected person.

This spurs a great need to study the transmission of this virus and find a suitable way to stop its transmission. Therefore, we can utilize one of the important tools of mathematics known as mathematical modeling to explore the details of the transmission. Many mathematical models have been developed in recent times. In [3], Li et al. proposed a latency-period pandemic COVID-19 model and adapted the proposed model to report the infected cases in mainland China. In [4], the authors developed a SIR-based COVID-19 infection model and implemented the proposed model to explore and forecast the transmission dynamics of this pandemic in China, Italy, and France, which are highly affected countries. In order to predict the COVID-19 infected cases in Brazil, Ribeiro et al. [5] developed a regression model. In [6], Ndairou et al. employed a super-spreader infected class transmission model and applied its model to the identified infected cases of Wuhan.

One of the best tools to investigate the dynamics of this infectious disease is a fractional epidemic model, which relies on fractional order differential operators and is a generalization of integer derivatives. Models with fractional derivatives afford us a better degree of precision and are also proportional to the real data in the compression models [7–9]. A variety of fractional operators have been presented from time to time in the literature with various kernels. Some of the repeatedly applied fractional operators are Caputo [10,11], Caputo–Fabrizio (CF) [12], and Atangana–Baleanu (ABC) [13]. In spite of the fact that most of the COVID-19 models elaborated so far are relying on classical integer-order derivatives, a few can be found with fractional operators. For instance, the authors in [14] formulated a fractional COVID-19 model using the ABC operator and gave a better approximation of the reported cases in Wuhan. Abdo et al. [15] developed a classical COVID-19 model to fractional order model using Mittag-Leffler kernel; they investigated the existence, Ulam stability analysis, and simulation results. Many modelings of different real-world problems under different kinds of fractional derivatives can be found in [16–20].

Thus, we reformulated the considered model in [14] by applying the fractal fractional derivative in the frame of the Caputo operator with a power law. In [14], they studied the reported cases on 21 January 2020, through 28 January 2020, of Wuhan. Here, in this research paper, we consider the reported cases in the Kingdom of Saudi Arabia from 1 March 2020 till 30 March 2021, with a forecast calculation for April and May 2021. We have provided an excellent fit to the reported cases and then estimated the model parameters to explore the transmission dynamics 2 of this novel infection.

This work contains six sections. We present summarized details about the mathematical modeling of the COVID-19 in Section 2. In Section 3, we give some foundations related to advanced fractional calculus. The fundamental properties and qualitative analysis of the proposed model will be investigated in Section 4. In Section 5, we provide the numerical approach for the solution of the proposed model. Forecasts and statistical analysis are given in Section 6. Moreover, we give the numerical simulations in Section 7. Concluding remarks are offered in Section 8.

2. Formulation of the Model

The model background that we consider here in the frame of a fractal-fractional derivative is given below and can be seen in [14]

$$\begin{cases} D_t S_1 = \Lambda - \frac{\bar{\eta}(I_1+\bar{\psi}A_1)}{N} S_1 - \bar{\eta}_\iota M_1 S_1 - \upsilon S_1, \\ D_t E_1 = \frac{\bar{\eta}(I_1+\bar{\psi}A_1)}{N} S_1 + \bar{\eta}_\iota M_1 S_1 - (\bar{\Theta}\bar{\rho} + (1-\bar{\Theta})\iota + \upsilon) E_1, \\ D_t I_1 = (1-\bar{\Theta})\iota E_1 - (\bar{\chi} + \upsilon) I_1, \\ D_t A_1 = \bar{\Theta}\bar{\rho} E_1 - (\bar{\chi}_a + \upsilon) A_1, \\ D_t R_1 = \bar{\chi}_a A_1 + \bar{\chi} I_1 - \upsilon R_1, \\ D_t M_1 = \bar{\varrho} I_1 + \bar{\varpi} A_1 - \bar{\nu} M_1, \end{cases} \tag{1}$$

where $D_t = \frac{d}{dt}$. The corresponding initial conditions are

$$\begin{cases} S_1(t_0) = \bar{S}_0 \geq 0, E_1(t_0) = \bar{E}_0 \geq 0, I_1(t_0) = \bar{I}_0 \geq 0, \\ A_1(t_0) = \bar{A}_0 \geq 0, R_1(t_0) = \bar{R}_0 \geq 0, M_1(t_0) = \bar{M}_0 \geq 0. \end{cases} \tag{2}$$

In this model, the total human population is denoted by $\bar{N}(t)$ which is again divided into five categories and some parameters of this pandemic model are given as the following table

Compartments and Parameters	**Description**
$S_1(t)$	Susceptible class
$E_1(t)$	Exposed class
$I_1(t)$	Infected class
$A_1(t)$	In-transmutable infected people showing no clinical symptoms
$R_1(t)$	Recovered people
$M_1(t)$	COVID-19 in the first identified case
Λ	The birth rate
υ	The natural death rate
$\bar{\varrho}$	The rate of Transmutable infected people into M_1
$\bar{\varpi}$	The rate of in-transmutable infected people into M_1
$\bar{\nu}$	The rate of virus leaving in M_1 for the M_1 class
$1/\bar{\nu}$	The total life period of COVID-19 virus
$\bar{\eta}$	The disease transmission coefficient
$\bar{\psi}$	The transmittable multiple of A_1 to I_1 ($0 \leq \bar{\psi} \leq 1$)
$\bar{\eta}_\iota$	Infected people due to an interactivity M_1 with S_1
$\bar{\eta}_\omega$	The transmission rate from M_1 to S_1
ι	Transmission rate of the exposed persons the infection to I_1 after the incubation period
$\bar{\rho}$	Transmission rate of the exposed persons the infection to A_1 after the incubation period
$\bar{\Theta}$	In-transmutable infection
$1/\bar{\chi}$	The infectious period of transmutable I_1 persons
$1/\bar{\chi}_a$	The infectious period of in-transmutable A_1 persons

The susceptible people who get the infection after an effective contact with the people in I_1 and A_1 at the rate of $\frac{\bar{\eta}(I_1+\bar{\psi}A_1)S_1}{N}$.

Now, we shall reconsider the model (1) by including fractional order derivative $0 < \mu \leq 1$ and fractal dimension $0 < \chi \leq 1$ as follows

$$\begin{cases} {}^{FFP}\mathbb{D}_{0,t}^{\mu,\chi} S_1(t) = \Lambda - \frac{\bar{\eta}(I_1+\bar{\psi}A_1)}{N} S_1 - \bar{\eta}_\iota M_1 S_1 - \upsilon S_1, \\ {}^{FFP}\mathbb{D}_{0,t}^{\mu,\chi} E_1(t) = \frac{\bar{\eta}(I_1+\bar{\psi}A_1)}{N} S_1 + \bar{\eta}_\iota M_1 S_1 - (\bar{\Theta}\bar{\rho} + (1-\bar{\Theta})\iota + \upsilon) E_1, \\ {}^{FFP}\mathbb{D}_{0,t}^{\mu,\chi} I_1(t) = (1-\bar{\Theta})\iota E_1 - (\bar{\chi} + \upsilon) I_1, \\ {}^{FFP}\mathbb{D}_{0,t}^{\mu,\chi} A_1(t) = \bar{\Theta}\bar{\rho} E_1 - (\bar{\chi}_a + \upsilon) A_1, \\ {}^{FFP}\mathbb{D}_{0,t}^{\mu,\chi} R_1(t) = \bar{\chi}_a A_1 + \bar{\chi} I_1 - \upsilon R_1, \\ {}^{FFP}\mathbb{D}_{0,t}^{\mu,\chi} M_1(t) = \bar{\varrho} I_1 + \bar{\varpi} A_1 - \bar{\nu} M_1, \end{cases} \tag{3}$$

where ${}^{FFP}\mathbb{D}_{0,t}^{\mu,\chi}$ is the fractal-fractional derivative of order $0 < \mu \leq 1$ and fractal dimension $0 < \chi \leq 1$ in Caputo sense with power law. We must construct a model (3) by means of the derivative of fractal fractional order in Caputo sense with power law as it provides an extremely realistic result and possesses a greater degree of freedom than integer-order. Precisely, we consider model (3) possesses fractional-order μ and fractal dimension χ describing the situation that lies between two integer values. The result will be accomplished by having the whole density of every compartment converging faster at a low order.

3. Foundations

Let $\Delta = [0, T]$ $(T < \infty)$, and $\mathcal{U} = C(\Delta, \mathbb{R}^6)$ is a Banach space equipped with the norm given by

$$\|\Theta\| = \sup_{t\in\Delta}|\Theta(t)|, \text{ for } \Theta \in \mathcal{U},$$

where

$$|\Theta(t)| = |S_1(t) + E_1(t) + I_1(t) + A_1(t) + R_1(t) + M_1(t)|$$

and $S_1, E_1, I_1, A_1, R_1, M_1 \in C(\Delta, \mathbb{R})$.

Definition 1 ([21]). *Let $\Theta(t)$ is continuous differentiable in (a, b) with order χ. Then, the fractal-fractional derivative of Θ of order μ in the frame of Riemann–Liouville and Caputo with the power law are supplied by*

$${}^{FFP}D_{a,t}^{\mu,\chi}\Theta(t) = \frac{1}{\Gamma(n-\mu)}D_{t\chi}\int_a^t (t-\sigma)^{n-\mu-1}\Theta(\sigma)d\sigma, \quad n-1 < \mu \leq n, \quad 0 < n-1 < \chi \leq n$$

and

$${}^{FFP}D_{a,t}^{\mu,\chi}\Theta(t) = \frac{1}{\Gamma(n-\mu)}\int_a^t (t-\sigma)^{n-\mu-1}D_{t\chi}\Theta(\sigma)d\sigma, \quad n-1 < \mu \leq n, \quad 0 < n-1 < \chi \leq n$$

respectively, where $D_{t\chi}\Theta(t) = \lim_{t\to\sigma}\frac{\Theta(t)-\Theta(\sigma)}{t^\chi-\sigma^\chi}$.

Definition 2 ([21]). *Let $u(t)$ is continuous in (a, b). Then the fractal-fractional integral of u with order γ in the definition Riemann–Liouville with power law is given by*

$${}^{FFP}I_{a,t}^{\mu,\chi}\Theta(t) = \frac{\chi}{\Gamma(\mu)}\int_a^t \sigma^{\chi-1}(t-\sigma)^{\mu-1}\Theta(\sigma)d\sigma.$$

Lemma 1 ([21]). *If f is continuous on (a, b), then the following fractal FDE*

$${}^{FFP}D_{a,t}^{\mu,\chi}\Theta(t) = z(t)$$

has a unique solution

$$\Theta(t) = \Theta(a) + \frac{\chi}{\Gamma(\mu)}\int_a^t \sigma^{\chi-1}(t-\sigma)^{\mu-1}z(\sigma)d\sigma.$$

4. Qualitative Analysis of the Proposed COVID-19 Model

In this section, we discuss the positivity and equilibrium analysis of the model (3). Then we investigate the uniqueness, existence, and Hyers–Ulam–Rassias stability results of the proposed model.

4.1. Positivity of the Model (3)

For the positivity of the model solution, let us structure the following set:

$$\mathbb{R}_+^6 = \left\{z \in \mathbb{R}^6 : z \geq 0 \text{ and } z(t) = \left(\ S_1(t), E_1(t), I_1(t), A_1(t), R_1(t), M_1(t)\ \right)^T\right\}.$$

Theorem 1. *A solution $z(t)$ of the given fractal fractional model (3) exists and belongs to $\mathbb{R}^6_+$. Moreover, the solution will be non-negative.*

Proof. Form the model (3), we conclude that

$$\begin{cases} {}^{FFP}\mathbb{D}^{\mu,\chi}_{0,t} S_1(t)\Big|_{S_1=0} = \Lambda \geq 0, \\ {}^{FFP}\mathbb{D}^{\mu,\chi}_{0,t} E_1(t)\Big|_{E_1=0} = \left(\frac{\bar{\eta}(I_1+\bar{\psi}A_1)}{N} + \bar{\eta}_\iota M_1\right) S_1 \geq 0, \\ {}^{FFP}\mathbb{D}^{\mu,\chi}_{0,t} I_1(t)\Big|_{I_1=0} = (1-\bar{\Theta})\iota E_1 \geq 0, \\ {}^{FFP}\mathbb{D}^{\mu,\chi}_{0,t} A_1(t)\Big|_{A_1=0} = \bar{\Theta}\bar{\rho}E_1 \geq 0, \\ {}^{FFP}\mathbb{D}^{\mu,\chi}_{0,t} R_1(t)\Big|_{R_1=0} = \bar{\chi}_a A_1 + \bar{\chi} I_1 \geq 0, \\ {}^{FFP}\mathbb{D}^{\mu,\chi}_{0,t} M_1(t)\Big|_{M_1=0} = \bar{\varrho} I_1 + \bar{\varpi} A_1 \geq 0. \end{cases} \tag{4}$$

Consequently, we infer that the solution will remain in $\mathbb{R}^6_+$ for all $t \geq 0$. The total dynamics of the individuals can be acquired by the first five equations of the model (3) which gives

$${}^{FFP}D^{\mu,\chi}_{0,t}\bar{N}(t) = \Lambda - v\bar{N}(t)$$

or

$${}^{RL}D^{\mu}_{0,t}\bar{N}(t) = \chi t^{\chi-1}(\Lambda - v\bar{N}(t))$$

By replacing ${}^{Rt}\mathrm{D}^{\mu}_{0,t}$ with ${}^{C}\mathrm{D}^{\mu}_{0,t}$ and applying the Laplace transform, we get

$$\bar{N}(t) = E_{\mu,1}(-vt^\mu)\bar{N}(0) + \Lambda\Gamma(\chi+1)t^{\chi+\mu-1}E_{\mu,\chi+\mu}(-vt^\mu),$$

where $E_{\mu,\nu}$ is called the Mittag-Leffler function. Taking into account the fact that $E_{\mu,\nu}$ has asymptotic behavior [10]; therefore, we get $\lim_{t\to\infty}\bar{N}(t) \leq \frac{\Lambda}{v}$. The feasible region for model (3) is structured as:

$$\mathcal{A} = \left\{(S_1, E_1, I_1, A_1, R_1, M_1) \in \mathbb{R}^6 : S_1, E_1, I_1, A_1, R_1, M_1 \geq 0 \text{ and } \bar{N}(t) \leq \frac{\Lambda}{v}\right\}.$$

□

4.2. Equilibrium Points

The model (3) possesses two equilibrium points: Disease Free Equilibrium (DFE) and Endemic Equilibrium (EE). Equating the fractal fractional COVID-19 model to zero as follows:

$$\begin{aligned} {}^{FFP}\mathbb{D}^{\mu,\chi}_{0,t} S_1(t) &= \Lambda - \frac{\bar{\eta}(I_1+\bar{\psi}A_1)}{N}S_1 - \bar{\eta}_\iota M_1 S_1 - vS_1 = 0, \\ {}^{FFP}\mathbb{D}^{\mu,\chi}_{0,t} E_1(t) &= \frac{\bar{\eta}(I_1+\bar{\psi}A_1)}{N}S_1 + \bar{\eta}_\iota M_1 S_1 - (\bar{\Theta}\bar{\rho} + (1-\bar{\Theta})\iota + v)E_1 = 0, \\ {}^{FFP}\mathbb{D}^{\mu,\chi}_{0,t} I_1(t) &= (1-\bar{\Theta})\iota E_1 - (\bar{\chi}+v)I_1 = 0, \\ {}^{FFP}\mathbb{D}^{\mu,\chi}_{0,t} A_1(t) &= \bar{\Theta}\bar{\rho}E_1 - (\bar{\chi}_a+v)A_1 = 0, \\ {}^{FFP}\mathbb{D}^{\mu,\chi}_{0,t} R_1(t) &= \bar{\chi}_a A_1 + \bar{\chi} I_1 - vR_1 = 0, \\ {}^{FFP}\mathbb{D}^{\mu,\chi}_{0,t} M_1(t) &= \bar{\varrho} I_1 + \bar{\varpi} A_1 - \bar{v} M_1 = 0. \end{aligned}$$

Thus, the point $\mathcal{D}_0 = (S^0_1, 0, 0, 0, 0, 0) = (\Lambda/v, 0, 0, 0, 0, 0)$ is the DFE.

To compute the basic reproduction number for the proposed model (3), we refer to [22].

In addition, by utilizing the next generation approach we get the following equation for the basic reproduction number:

$$\mathcal{R}_0 = \mathcal{R}_1 + \mathcal{R}_2$$

where

$$\mathcal{R}_1 = \frac{\bar{\Theta}\bar{\rho}(\bar{\nu}\bar{\psi}\bar{\eta}\upsilon + \Lambda\bar{\omega}\bar{\eta}_\iota)}{\bar{\nu}\upsilon(\bar{\Theta}\bar{\rho} + (1-\bar{\Theta})\iota + \upsilon)(\bar{\chi}_a + \upsilon)},$$

and

$$\mathcal{R}_2 = \frac{(1-\bar{\Theta})\iota(\bar{\nu}\bar{\eta}\upsilon + \Lambda\bar{\varrho}\bar{\eta}_\iota)}{\bar{\nu}\upsilon(\bar{\Theta}\bar{\rho} + (1-\bar{\Theta})\iota + \upsilon)(\bar{\chi} + \upsilon)}.$$

The following theorem provides us with the necessary part.

Theorem 2. *The DFE $\mathcal{D}_0$ of the model (3) is locally asymptotically stable if ($\mathcal{R}_0 < 1$) for all eigenvalues λ_i of the Jacobian matrix $J_{\mathcal{D}_0}$ of the model (3) satisfy*

$$|\arg(\lambda_i)| > \frac{\mu\pi}{2}, i = 1, 2, 3, 4. \tag{5}$$

Proof. The Jacobian and linearization matrix is defined by:

$$J_{\mathcal{D}_0} = \begin{pmatrix} -\upsilon & 0 & -\bar{\eta} & -\bar{\eta}\bar{\psi} & 0 & -\frac{\bar{\eta}_\iota\bar{\nu}}{\upsilon} \\ 0 & -k_1 & \bar{\eta} & \bar{\eta}\bar{\psi} & 0 & \frac{\bar{\eta}_\iota\bar{\nu}}{\bar{\nu}} \\ 0 & (1-\bar{\Theta})\iota & -k_2 & 0 & 0 & 0 \\ 0 & \bar{\Theta}_{\bar{\rho}} & 0 & -k_3 & 0 & 0 \\ 0 & 0 & \bar{\chi} & \bar{\chi}_a & -\upsilon & 0 \\ 0 & 0 & \bar{\varrho} & \bar{\omega} & 0 & -\bar{\nu} \end{pmatrix}$$

where $k_1 = (\bar{\Theta}\bar{\rho} + (1-\bar{\Theta})\iota + \upsilon)$, $k_2 = (\bar{\chi} + \upsilon)$, and $k_3 = (\bar{\chi}_a + \upsilon)$.

The characteristic equation in terms of λ_i for $J_{\mathcal{D}_0}$ is defined below:

$$(\lambda + \upsilon)^2(\lambda^4 + a_1\lambda^3 + a_2\lambda^2 + a_3\lambda + a_4) = 0, \tag{6}$$

where

$$a_1 = k_1 + k_2 + k_3 + \bar{\nu},$$
$$a_2 = (k_1k_3 - \bar{\eta}\bar{\Theta}\bar{\rho}\bar{\psi}) + (k_1k_2 - \bar{\eta}(1-\bar{\Theta})\iota) + (k_1 + k_2 + k_3)\bar{\nu} + k_2k_3,$$
$$a_3 = \bar{\nu}k_1[k_3(1-\mathcal{R}_1) + k_2(1-\mathcal{R}_2)] + k_2[\bar{\nu}(k_3 - \bar{\eta}\bar{\Theta}\bar{\rho}\bar{\psi})] + \bar{\Theta}\iota k_3 + k_3(k_1k_2 - \bar{\eta}\iota),$$
$$a_4 = \bar{\nu}k_1k_2k_3(1-\mathcal{R}_0).$$

From (6), we get that the given eigenvalues $-\upsilon$ must assure the condition in (5) for all $\mu \in (0, 1)$. In addition, we know that if $\mathcal{R}_0 < 1$, then for all $a_i > 0$, and $a_1a_2a_3 > a_3^2 + a_1^2a_4$ can be easily met by using the above coefficients. So, the model (3) at the DFE is locally asymptotically stable if $\mathcal{R}_0 < 1$.

For the EE of the model (3), we denote it by $\mathcal{D}^*$, and $\mathcal{D}^* = (S_1^*, E_1^*, I_1^*, A_1^*, R_1^*, M_1^*)$, given by

$$\begin{cases} S_1^* = \frac{\Lambda}{\bar{\lambda}^* + \upsilon}, \\ E_1^* = \frac{\bar{\lambda}^* S_1^*}{k_1}, \\ I_1^* = \frac{(1-\bar{\Theta})\iota}{k_1} E_1^*, \\ A_1^* = \frac{\bar{\Theta}\bar{\rho}}{k_2} E_1^*, \\ R_1^* = \frac{\bar{\chi}_a A_1^* + \bar{\chi} I_1^*}{\upsilon}, \\ M_1^* = \frac{\bar{\omega} A_1^* + \bar{\varrho} I_1^*}{\bar{\nu}}, \end{cases}$$

where

$$\bar{\lambda}^* = \frac{\bar{\eta}\left(I_1^* + \bar{\psi}A_1^*\right)}{S_1^* + E_1^* + I_1^* + A_1^* + R_1^*} + \bar{\eta}_\iota M_1^*,$$

which satisfies the following equation

$$P(\bar{\lambda}^*) = m_1(\bar{\lambda}^*)^2 + m_2\bar{\lambda}^* \tag{7}$$

The coefficients in (7) are $m_1 = \bar{\nu}k_1k_2k_3$, and $m_2 = \bar{\nu}\upsilon k_1k_2k_3(1-\mathcal{R}_0)$.

Obviously, $m_1 > 0$ and $m_2 \geq 0$ if $\mathcal{R}_0 < 1$, and $\bar{\lambda}^* = -\frac{m_2}{m_1} \leq 0$. Hence, no EE will exist if $\mathcal{R}_0 < 1$. □

4.3. Existence and Uniqueness Results

To begin with, we will express the differentiation in the model (3) as integrals, that is

$$\begin{cases} \frac{1}{\Gamma(1-\mu)}\frac{d}{dt^\chi}\int_0^t (t-\sigma)^{-\mu}S_1(\sigma)d\sigma = \Lambda - \frac{\bar{\eta}(I_1+\bar{\psi}A_1)}{N}S_1 - \bar{\eta}_\iota M_1S_1 - \upsilon S_1, \\ \frac{1}{\Gamma(1-\mu)}\frac{d}{dt^\chi}\int_0^t (t-\sigma)^{-\mu}E_1(\sigma)d\sigma = \frac{\bar{\eta}(I_1+\bar{\psi}A_1)}{N}S_1 + \bar{\eta}_\iota M_1S_1 - k_1E_1, \\ \frac{1}{\Gamma(1-\mu)}\frac{d}{dt^\chi}\int_0^t (t-\sigma)^{-\mu}I_1(\sigma)d\sigma = (1-\bar{\Theta})\iota E_1 - k_2I_1, \\ \frac{1}{\Gamma(1-\mu)}\frac{d}{dt^\chi}\int_0^t (t-\sigma)^{-\mu}A_1(\sigma)d\sigma = \bar{\Theta}\bar{\rho}E_1 - k_3A_1, \\ \frac{1}{\Gamma(1-\mu)}\frac{d}{dt^\chi}\int_0^t (t-\sigma)^{-\mu}R_1(\sigma)d\sigma = \bar{\chi}_a A_1 + \bar{\chi}I_1 - \upsilon R_1, \\ \frac{1}{\Gamma(1-\mu)}\frac{d}{dt^\chi}\int_0^t (t-\sigma)^{-\mu}M_1(\sigma)d\sigma = \bar{\varrho}I_1 + \bar{\varpi}A_1 - \bar{\nu}M_1. \end{cases} \tag{8}$$

Due to the integrals in the model (8) being differentiable, we can formulate the model (8) as

$$\begin{cases} {}^{RL}D_{0,t}^{\mu}S_1(t) = \chi t^{\chi-1}\mathcal{K}_1(t, S_1(t), E_1(t), I_1(t), A_1(t), R_1(t), M_1(t)), \\ {}^{RL}D_{0,t}^{\mu}E_1(t) = \chi t^{\chi-1}\mathcal{K}_2(t, S_1(t), E_1(t), I_1(t), A_1(t), R_1(t), M_1(t)), \\ {}^{RL}D_{0,t}^{\mu}I_1(t) = \chi t^{\chi-1}\mathcal{K}_3(t, S_1(t), E_1(t), I_1(t), A_1(t), R_1(t), M_1(t)), \\ {}^{RL}D_{0,t}^{\mu}A_1(t) = \chi t^{\chi-1}\mathcal{K}_4(t, S_1(t), E_1(t), I_1(t), A_1(t), R_1(t), M_1(t)), \\ {}^{RL}D_{0,t}^{\mu}R_1(t) = \chi t^{\chi-1}\mathcal{K}_5(t, S_1(t), E_1(t), I_1(t), A_1(t), R_1(t), M_1(t)), \\ {}^{RL}D_{0,t}^{\mu}M_1(t) = \chi t^{\chi-1}\mathcal{K}_6(t, S_1(t), E_1(t), I_1(t), A_1(t), R_1(t), M_1(t)), \end{cases} \tag{9}$$

where

$$\begin{cases} \mathcal{K}_1(t, S_1, E_1, I_1, A_1, R_1, M_1) = \Lambda - \frac{\bar{\eta}(I_1+\bar{\psi}A_1)}{N}S_1 - \bar{\eta}_\iota M_1S_1 - \upsilon S_1, \\ \mathcal{K}_2(t, S_1, E_1, I_1, A_1, R_1, M_1) = \frac{\bar{\eta}(I_1+\bar{\psi}A_1)}{N}S_1 + \bar{\eta}_\iota M_1S_1 - k_1E_1, \\ \mathcal{K}_3(t, S_1, E_1, I_1, A_1, R_1, M_1) = (1-\bar{\Theta})\iota E_1 - k_2I_1, \\ \mathcal{K}_4(t, S_1, E_1, I_1, A_1, R_1, M_1) = \bar{\Theta}\bar{\rho}E_1 - k_3A_1, \\ \mathcal{K}_5(t, S_1, E_1, I_1, A_1, R_1, M_1) = \bar{\chi}_a A_1 + \bar{\chi}I_1 - \upsilon R_1, \\ \mathcal{K}_6(t, S_1, E_1, I_1, A_1, R_1, M_1) = \bar{\varrho}I_1 + \bar{\varpi}A_1 - \bar{\nu}M_1. \end{cases}$$

By replacing ${}^{RL}D_{0,t}^{\mu}$ with ${}^{C}D_{0,t}^{\mu}$ then applying the initial conditions and fractional integral operator, we turn model (9) into the following integral equations:

$$\begin{cases} S_1(t) = S_1(0) + \frac{1}{\Gamma(\mu)}\int_0^t \chi\sigma^{\chi-1}(t-\sigma)^{\mu-1}\mathcal{K}_1(\sigma, S_1, E_1, I_1, A_1, R_1, M_1)d\sigma, \\ E_1(t) = E_1(0) + \frac{1}{\Gamma(\mu)}\int_0^t \chi\sigma^{\chi-1}(t-\sigma)^{\mu-1}\mathcal{K}_2(\sigma, S_1, E_1, I_1, A_1, R_1, M_1)d\sigma, \\ I_1(t) = I_1(0) + \frac{1}{\Gamma(\mu)}\int_0^t \chi\sigma^{\chi-1}(t-\sigma)^{\mu-1}\mathcal{K}_3(\sigma, S_1, E_1, I_1, A_1, R_1, M_1)d\sigma, \\ A_1(t) = A_1(0) + \frac{1}{\Gamma(\mu)}\int_0^t \chi\sigma^{\chi-1}(t-\sigma)^{\mu-1}\mathcal{K}_4(\sigma, S_1, E_1, I_1, A_1, R_1, M_1)d\sigma, \\ R_1(t) = R_1(0) + \frac{1}{\Gamma(\mu)}\int_0^t \chi\sigma^{\chi-1}(t-\sigma)^{\mu-1}\mathcal{K}_5(\sigma, S_1, E_1, I_1, A_1, R_1, M_1)d\sigma, \\ M_1(t) = M_1(0) + \frac{1}{\Gamma(\mu)}\int_0^t \chi\sigma^{\chi-1}(t-\sigma)^{\mu-1}\mathcal{K}_6(\sigma, S_1, E_1, I_1, A_1, R_1, M_1)d\sigma. \end{cases} \tag{10}$$

To prove the qualitative properties of the solution for model (3), we make use of the fixed point technique and the Picard–Lindel'f approach. First, we reformulate the model (3) which takes the form:

$$\begin{cases} {}^{FFP}\mathbb{D}_{0,t}^{\mu,\chi}\Theta(t) = \mathcal{K}(t,\Theta(t)), \ \ 0 < \mu, \chi \leq 1, \\ \Theta(0) = \Theta_0 \geq 0, \quad 0 < t < T < \infty, \end{cases} \tag{11}$$

where

$$\Theta(t) = \begin{pmatrix} S_1(t) \\ E_1(t) \\ I_1(t) \\ A_1(t) \\ R_1(t) \\ M_1(t) \end{pmatrix}, \ \ \Theta(0) = \begin{pmatrix} S_1(0) = S_0 \\ E_1(0) = E_0 \\ I_1(0) = I_0 \\ A_1(0) = A_0 \\ R_1(0) = R_0 \\ M_1(0) = M_0 \end{pmatrix} = \Theta_0$$

and

$$\mathcal{K}(t,\Theta(t)) = \begin{pmatrix} \mathcal{K}_1(t,S_1(t),E_1(t),I_1(t),A_1(t),R_1(t),M_1(t)) \\ \mathcal{K}_2(t,S_1(t),E_1(t),I_1(t),A_1(t),R_1(t),M_1(t)) \\ \mathcal{K}_3(t,S_1(t),E_1(t),I_1(t),A_1(t),R_1(t),M_1(t)) \\ \mathcal{K}_4(t,S_1(t),E_1(t),I_1(t),A_1(t),R_1(t),M_1(t)) \\ \mathcal{K}_5(t,S_1(t),E_1(t),I_1(t),A_1(t),R_1(t),M_1(t)) \\ \mathcal{K}_6(t,S_1(t),E_1(t),I_1(t),A_1(t),R_1(t),M_1(t)) \end{pmatrix}.$$

In view of Lemma 1, the system (11) gives

$$\Theta(t) = \Theta(0) + \frac{\chi}{\Gamma(\mu)}\int_0^t \sigma^{\tau-1}(t-\sigma)^{\mu-1}\mathcal{K}(\sigma,\Theta(\sigma))d\sigma.$$

Furthermore, $\mathcal{K}$ satisfies

$$|\mathcal{K}(\sigma,\Theta_1(\sigma)) - \mathcal{K}(\sigma,\Theta_2(\sigma))| \leq L_{\mathcal{K}}|\Theta_1(\sigma) - \Theta_2(\sigma)|, \ \ L_{\mathcal{K}} > 0. \tag{12}$$

Theorem 3 (Existence of unique solution). *Assume that the assumption (12) holds. Then the system (11) has a unique solution if* $\mathcal{P} := \frac{\chi\mathcal{B}(\mu,\chi)}{\Gamma(\mu)}T^{\chi+\mu-1}L_{\mathcal{K}} < 1$, *where* $\mathcal{B}(\cdot,\cdot)$ *is the beta function.*

Proof. Consider the Picard operator $\Pi : \mathcal{U} \to \mathcal{U}$ defined by

$$\Pi\Theta(t) = \Theta(0) + \frac{\chi}{\Gamma(\mu)}\int_0^t \sigma^{\tau-1}(t-\sigma)^{\mu-1}\mathcal{K}(\sigma,\Theta(\sigma))d\sigma, \tag{13}$$

and set $\sup_{\sigma\in\Delta}\mathcal{K}(\sigma,0) = \mathcal{K}_0$. It should be noted that the solution of the system (11) is bounded, i.e.,

$$\begin{aligned} \|\Pi\Theta - \Theta_0\| &= \sup_{t\in\Delta}|\Pi\Theta(t) - \Theta(0)| \\ &= \sup_{t\in\Delta}\left|\frac{\chi}{\Gamma(\mu)}\int_0^t \sigma^{\tau-1}(t-\sigma)^{\mu-1}\mathcal{K}(\sigma,\Theta(\sigma))d\sigma\right| \\ &\leq \sup_{t\in\Delta}\frac{\chi}{\Gamma(\mu)}\int_0^t \sigma^{\tau-1}(t-\sigma)^{\mu-1}|\mathcal{K}(\sigma,\Theta(\sigma))|d\sigma \\ &\leq \sup_{t\in\Delta}\frac{\chi}{\Gamma(\mu)}\int_0^t \sigma^{\tau-1}(t-\sigma)^{\mu-1}|\mathcal{K}(\sigma,\Theta(\sigma)) - \mathcal{K}(\sigma,0)|d\sigma \\ &\leq \frac{\chi\mathcal{B}(\mu,\chi)}{\Gamma(\mu)}t^{\chi+\mu-1}(L_{\mathcal{K}}\|\Theta\|_\infty + \mathcal{K}_0) \\ &\leq \frac{\chi\mathcal{B}(\mu,\chi)}{\Gamma(\mu)}T^{\chi+\mu-1}(L_{\mathcal{K}}\|\Theta\|_\infty + \mathcal{K}_0) := \mathcal{R} < \infty. \end{aligned}$$

Now, using Picard operator (13) with given any $\Theta_1, \Theta_2 \in \mathcal{U}$, we obtain

$$\begin{aligned}
\|\Pi\Theta_1 - \Pi\Theta_2\| &= \sup_{t\in\Delta}|\Pi\Theta_1(t) - \Pi\Theta_2(t)| \\
&\leq \sup_{t\in\Delta}\frac{\chi}{\Gamma(\mu)}\int_0^t \sigma^{\tau-1}(t-\sigma)^{\mu-1}|\mathcal{K}(\sigma,\Theta_1(\sigma)) - \mathcal{K}(\sigma,\Theta_1(\sigma))|d\sigma \\
&\leq \sup_{t\in\Delta}\frac{\chi}{\Gamma(\mu)}\int_0^t \sigma^{\tau-1}(t-\sigma)^{\mu-1}L_{\mathcal{K}}|\Theta_1(\sigma) - \Theta_2(\sigma)|d\sigma \\
&\leq \frac{\chi\mathcal{B}(\mu,\chi)}{\Gamma(\mu)}t^{\chi+\mu-1}L_{\mathcal{K}}\|\Theta_1 - \Theta_2\| \\
&\leq \frac{\chi\mathcal{B}(\mu,\chi)}{\Gamma(\mu)}T^{\chi+\mu-1}L_{\mathcal{K}}\|\Theta_1 - \Theta_2\|,
\end{aligned}$$

which implies that$\|\Pi\Theta_1 - \Pi\Theta_2\| \leq \mathcal{P}\|\Theta_1 - \Theta_2\|$. Thus Π is a contraction, and hence model (11) has a unique solution due to Banach contraction principle [23]. □

4.4. Stability Results

In this part, we discuss the stability of Ulam–Hyers and Ulam–Hyers–Rassias for the considered model (11). Furthermore, since stability is essential for approximate solution, we intend to use nonlinear functional analysis on these types of stability for the given model.

Definition 3. *Let* $0 < \mu, \chi \leq 1$ *and* $\mathcal{K} \in C\big(\Delta \times \mathbb{R}^6, \mathbb{R}\big)$. *Then (11) is referred to Hyers–Ulam stable if there exist* $\epsilon, C_{\mathcal{K}} > 0$ *such that, for each solution* $\widetilde{\Theta} \in \mathcal{U}$ *satisfies*

$$\left|{}^{FFP}D_{0,t}^{\mu,\chi}\widetilde{\Theta}(t) - \mathcal{K}(t,\widetilde{\Theta}(t))\right| \leq \epsilon, \ \ \forall t \in \Delta, \tag{14}$$

there exists a solution $\Theta \in \mathcal{U}$ *of (11) with*

$$\left|\widetilde{\Theta}(t) - \Theta(t))\right| \leq \epsilon C_{\mathcal{K}}, \ \ \forall t \in \Delta,$$

where $\epsilon = \max(\epsilon_j)^T$ *and* $C_{\mathcal{K}} = \max(C_{\mathcal{K}_j})^T, j = 1, 2, \ldots, 6$.

Definition 4. *Let* $0 < \mu, \chi \leq 1$, $\mathcal{K} \in C\big(\Delta \times \mathbb{R}^6, \mathbb{R}\big)$ *and* $\varphi \in C(\Delta, \mathbb{R}^+)$. *Then (11) is referred to Hyers–Ulam–Rassias stable if there exists* $C_{\mathcal{K},\varphi} > 0$ *such that, for each solution* $\widetilde{\Theta} \in \mathcal{U}$ *satisfies*

$$\left|{}^{FFP}D_{0,t}^{\mu,\chi}\widetilde{\Theta}(t) - \mathcal{K}(t,\widetilde{\Theta}(t))\right| \leq \epsilon\varphi(t), \ \ \forall t \in \Delta, \tag{15}$$

there exists a solution $\Theta \in \mathcal{U}$ *of (11) with*

$$\left|\widetilde{\Theta}(t) - \Theta(t))\right| \leq C_{\mathcal{K},\varphi}\epsilon\varphi(t), \ \ \forall t \in \Delta,$$

where $C_{\mathcal{K},\varphi} = \max(C_{\mathcal{K}_j,\varphi_j})^T$ *and* $\varphi = \max(\varphi_j)^T, j = 1, 2, \ldots, 6$.

Remark 1. *Let* $\epsilon > 0$. *Then the function* $\widetilde{\Theta} \in \mathcal{U}$ *satisfies (14) if and only if there exists a function* $\delta(t) \in \mathcal{U}$ *red satisfies the properties below:*

(i) $|\delta(t)| \leq \epsilon$, *for* $t \in \Delta$,
(ii) ${}^{FFP}D_{0,t}^{\mu,\chi}\widetilde{\Theta}(t) = \mathcal{K}(t,\widetilde{\Theta}(t)) + \delta(t), \ t \in \Delta, \delta = \max(\delta_j)^T, j = 1, 2, \ldots, 6$.

Remark 2. *Let* $\varphi \in C(\Delta, \mathbb{R}^+)$. *Then the function* $\widetilde{\Theta} \in \mathcal{U}$ *satisfies (15) if and only if there exists a function* $\delta^*(t) \in \mathcal{U}$ *with the property below:*

(i) $|\delta^*(t)| \leq \epsilon\varphi(t)$, *for* $t \in \Delta$,
(ii) ${}^{FFP}D_{0,t}^{\mu,\chi}\widetilde{\Theta}(t) = \mathcal{K}(t,\widetilde{\Theta}(t)) + \delta^*(t), \ t \in \Delta, \delta^* = \max(\delta_j^*)^T, j = 1, 2, \ldots, 6$.

Lemma 2. *$\widetilde{\Theta} \in \mathcal{U}$ satisfies (14) if $\widetilde{\Theta}$ satisfies the integral inequality given by*

$$\left|\widetilde{\Theta}(t) - \widetilde{\Theta}(0) - {}^{FFP}I_{0,t}^{\mu,\chi}\mathcal{K}(t,\widetilde{\Theta}(t))\right| \leq \Upsilon\epsilon,$$

where $\Upsilon := \frac{\chi T^{\chi+\mu-1}}{\Gamma(\mu)}\mathcal{B}(\chi,\mu)$.

Proof. According to (ii) of Remark 1 with Theorem 3, the system

$$\begin{aligned} {}^{FFP}D_{0,t}^{\mu,\chi}\widetilde{\Theta}(t) &= \mathcal{K}(t,\widetilde{\Theta}(t)) + \delta(t),\ t \in \Delta \\ \widetilde{\Theta}(0) &= \Theta_0 \geq 0. \end{aligned}$$

has a unique solution

$$\widetilde{\Theta}(t) = \widetilde{\Theta}(0) + {}^{FFP}I_{0,t}^{\mu,\chi}\Big[\mathcal{K}(t,\widetilde{\Theta}(t)) + \delta(t)\Big].$$

It follows from (i) of Remark 1 that

$$\begin{aligned} \left|\widetilde{\Theta}(t) - \widetilde{\Theta}(0) - {}^{FFP}I_{0,t}^{\mu,\chi}\mathcal{K}(t,\widetilde{\Theta}(t))\right| &= \left|{}^{FFP}I_{0,t}^{\mu,\chi}\delta(t)\right| \\ &\leq \frac{\chi}{\Gamma(\mu)}\int_0^t \sigma^{\chi-1}(t-\sigma)^{\mu-1}|\delta(\sigma)|d\sigma \\ &\leq \frac{\chi\epsilon}{\Gamma(\mu)}\int_0^t \sigma^{\chi-1}(t-\sigma)^{\mu-1}d\sigma \\ &= \left(\frac{\chi t^{\mu+\chi-1}}{\Gamma(\mu)}\mathcal{B}(\chi,\mu)\right)\epsilon \leq \Upsilon\epsilon. \end{aligned}$$

□

Theorem 4. *Suppose $\mathcal{K} \in C(\Delta \times \mathbb{R}^6, \mathbb{R})$ and (12) holds with $1 - \Upsilon L_{\mathcal{K}} > 0$. Then (11) is Ulam–Hyers stable.*

Proof. Let $\widetilde{\Theta} \in \mathcal{U}$ satisfies (15) and $\Theta \in \mathcal{U}$ be a unique solution of (11). Then, for any $\epsilon > 0$, $t \in \Delta$ and Lemma 2, we obtain

$$\begin{aligned} \left\|\widetilde{\Theta} - \Theta\right\| &= \sup_{t\in\Delta}\left|\widetilde{\Theta}(t) - \Theta(t)\right| \\ &= \sup_{t\in\Delta}\left|\widetilde{\Theta}(t) - \Theta_0 - {}^{FFP}I_{0,t}^{\mu,\chi}\mathcal{K}(t,\Theta(t))\right| \\ &\leq \sup_{t\in\Delta}\left|\widetilde{\Theta}(t) - \Theta_0 - {}^{FFP}I_{0,t}^{\mu,\chi}\mathcal{K}(t,\widetilde{\Theta}(t))\right| \\ &\quad + \sup_{t\in\Delta}{}^{FFP}I_{0,t}^{\mu,\chi}\left|\mathcal{K}(t,\widetilde{\Theta}(t)) - \mathcal{K}(t,\Theta(t))\right| \\ &\leq \Upsilon\epsilon + \frac{\chi}{\Gamma(\mu)}\int_0^t \sigma^{\tau-1}(t-\sigma)^{\mu-1}L_{\mathcal{K}}\left|\widetilde{\Theta}(\sigma) - \Theta(\sigma)\right|d\sigma \\ &\leq \Upsilon\epsilon + \Upsilon L_{\mathcal{K}}\left\|\widetilde{\Theta} - \Theta\right\|, \end{aligned}$$

which implies

$$\left\|\widetilde{\Theta} - \Theta\right\| \leq C_{\mathcal{K}}\epsilon,$$

where $C_{\mathcal{K}} := \frac{\Upsilon}{1-\Upsilon L_{\mathcal{K}}}$. □

Theorem 5. *Let $\mathcal{K} \in C(\Delta \times \mathbb{R}^6, \mathbb{R})$ satisfies (12), and $\varphi \in C(\Delta, \mathbb{R}^+)$ be an increasing function such that*

$$^{FFP}I_{0,t}^{\mu,\chi}\varphi(t) \leq C_\varphi \varphi(t), \quad C_\varphi > 0. \tag{16}$$

Then (11) is Ulam–Hyers–Rassias stable with respect to φ on Δ provided that $1 - \Upsilon L_{\mathcal{K}} > 0$.

Proof. In view of Theorem 3, the system (11) has the unique solution $\Theta \in \mathcal{U}$, that is

$$\Theta(t) = \Theta_0 + \frac{\chi}{\Gamma(\mu)} \int_0^t \sigma^{\tau-1}(t-\sigma)^{\mu-1}\mathcal{K}(\sigma, \Theta(\sigma))d\sigma, \quad t \in \Delta.$$

From (15) and keeping in mind (16), we have

$$\left|\widetilde{\Theta}(t) - \widetilde{\Theta}(0) - {}^{FFP}I_{0,t}^{\mu,\chi}\mathcal{K}(t, \widetilde{\Theta}(t))\right| \leq \epsilon C_\varphi \varphi(t).$$

Hence

$$\begin{aligned}
\left|\widetilde{\Theta}(t) - \Theta(t)\right| &= \left|\widetilde{\Theta}(t) - \Theta_0 - {}^{FFP}I_{0,t}^{\mu,\chi}\mathcal{K}(t, \Theta(t))\right| \\
&\leq \left|\widetilde{\Theta}(t) - \Theta_0 - {}^{FFP}I_{0,t}^{\mu,\chi}\mathcal{K}(t, \widetilde{\Theta}(t))\right| \\
&\quad + {}^{FFP}I_{0,t}^{\mu,\chi}\left|\mathcal{K}(t, \widetilde{\Theta}(t)) - \mathcal{K}(t, \Theta(t))\right| \\
&\leq \epsilon C_\varphi \varphi(t) + \frac{\chi}{\Gamma(\mu)} \int_0^t \sigma^{\tau-1}(t-\sigma)^{\mu-1} L_{\mathcal{K}} \left|\widetilde{\Theta}(\sigma) - \Theta(\sigma)\right| d\sigma \\
&\leq \epsilon C_\varphi \varphi(t) + \Upsilon L_{\mathcal{K}} \left|\widetilde{\Theta}(t) - \Theta(t)\right|
\end{aligned}$$

which implies

$$\left|\widetilde{\Theta}(t) - \Theta(t)\right| \leq \epsilon C_{\mathcal{K},\varphi} \varphi(t), \tag{17}$$

where $C_{\mathcal{K},\varphi} := \frac{C_\varphi}{1-\Upsilon L_{\mathcal{K}}}$. □

It is clear that when $\varphi(t) = 1$ in (17), the Ulam–Hyers stability result is obtained.

5. Numerical Scheme

In this section, we present a numerical approach for the solution of the model (3) by relying upon the procedure described in [21,24]. By using the systems (8)–(10) at the point $t_{\kappa+1}$, we obtain

$$\begin{cases}
S_{\kappa+1}(t) = \bar{S}_0 + \frac{\chi}{\Gamma(\mu)} \int_0^{t_{\kappa+1}} \sigma^{\chi-1}(t_{\kappa+1}-\sigma)^{\mu-1}\mathcal{K}_1(\sigma, S_1, E_1, I_1, A_1, R_1, M_1)d\sigma, \\
E_{\kappa+1}(t) = \bar{E}_0 + \frac{\chi}{\Gamma(\mu)} \int_0^{t_{\kappa+1}} \sigma^{\chi-1}(t_{\kappa+1}-\sigma)^{\mu-1}\mathcal{K}_2(\sigma, S_1, E_1, I_1, A_1, R_1, M_1)d\sigma, \\
I_{\kappa+1}(t) = \bar{I}_0 + \frac{\chi}{\Gamma(\mu)} \int_0^{t_{\kappa+1}} \sigma^{\chi-1}(t_{\kappa+1}-\sigma)^{\mu-1}\mathcal{K}_3(\sigma, S_1, E_1, I_1, A_1, R_1, M_1)d\sigma, \\
A_{\kappa+1}(t) = \bar{A}_0 + \frac{\chi}{\Gamma(\mu)} \int_0^{t_{\kappa+1}} \sigma^{\chi-1}(t_{\kappa+1}-\sigma)^{\mu-1}\mathcal{K}_4(\sigma, S_1, E_1, I_1, A_1, R_1, M_1)d\sigma, \\
R_{\kappa+1}(t) = \bar{R}_0 + \frac{\chi}{\Gamma(\mu)} \int_0^{t_{\kappa+1}} \sigma^{\chi-1}(t_{\kappa+1}-\sigma)^{\mu-1}\mathcal{K}_5(\sigma, S_1, E_1, I_1, A_1, R_1, M_1)d\sigma, \\
M_{\kappa+1}(t) = \bar{M}_0 + \frac{\chi}{\Gamma(\mu)} \int_0^{t_{\kappa+1}} \sigma^{\chi-1}(t_{\kappa+1}-\sigma)^{\mu-1}\mathcal{K}_6(\sigma, S_1, E_1, I_1, A_1, R_1, M_1)d\sigma.
\end{cases} \tag{18}$$

Then we approximate the integrals obtained in (18) to

$$\begin{cases}
S_{\kappa+1}(t) = \bar{S}_0 + \frac{\chi}{\Gamma(\mu)} \sum_{\ell=0}^{\kappa} \int_{t_\ell}^{t_{\ell+1}} \sigma^{\chi-1}(t_{\kappa+1}-\sigma)^{\mu-1}\mathcal{K}_1(\sigma, S_1, E_1, I_1, A_1, R_1, M_1)d\sigma, \\
E_{\kappa+1}(t) = \bar{E}_0 + \frac{\chi}{\Gamma(\mu)} \sum_{\ell=0}^{\kappa} \int_{t_\ell}^{t_{\ell+1}} \sigma^{\chi-1}(t_{\kappa+1}-\sigma)^{\mu-1}\mathcal{K}_2(\sigma, S_1, E_1, I_1, A_1, R_1, M_1)d\sigma, \\
I_{\kappa+1}(t) = \bar{I}_0 + \frac{\chi}{\Gamma(\mu)} \sum_{\ell=0}^{\kappa} \int_{t_\ell}^{t_{\ell+1}} \sigma^{\chi-1}(t_{\kappa+1}-\sigma)^{\mu-1}\mathcal{K}_3(\sigma, S_1, E_1, I_1, A_1, R_1, M_1)d\sigma, \\
A_{\kappa+1}(t) = \bar{A}_0 + \frac{\chi}{\Gamma(\mu)} \sum_{\ell=0}^{\kappa} \int_{t_\ell}^{t_{\ell+1}} \sigma^{\chi-1}(t_{\kappa+1}-\sigma)^{\mu-1}\mathcal{K}_4(\sigma, S_1, E_1, I_1, A_1, R_1, M_1)d\sigma, \\
R_{\kappa+1}(t) = \bar{R}_0 + \frac{\chi}{\Gamma(\mu)} \sum_{\ell=0}^{\kappa} \int_{t_\ell}^{t_{\ell+1}} \sigma^{\chi-1}(t_{\kappa+1}-\sigma)^{\mu-1}\mathcal{K}_5(\sigma, S_1, E_1, I_1, A_1, R_1, M_1)d\sigma, \\
M_{\kappa+1}(t) = \bar{M}_0 + \frac{\chi}{\Gamma(\mu)} \sum_{\ell=0}^{\kappa} \int_{t_\ell}^{t_{\ell+1}} \sigma^{\chi-1}(t_{\kappa+1}-\sigma)^{\mu-1}\mathcal{K}_6(\sigma, S_1, E_1, I_1, A_1, R_1, M_1)d\sigma.
\end{cases} \tag{19}$$

On $[t_\ell, t_{\ell+1}]$, we approximate the expression $\sigma^{\chi-1}\mathcal{K}_i(\sigma, S_1, E_1, I_1, A_1, R_1, M_1)$ where $i = 1, 2, 3, 4, 5, 6$ utilizing the Lagrangian piecewise interpolation as

$$\begin{aligned} Q_\ell^i(\sigma) &= \frac{\sigma - t_{\ell-1}}{t_\ell - t_{\ell-1}} t_\ell^{\chi-1}\mathcal{K}_i(t_\ell, S_\ell, E_\ell, I_\ell, A_\ell, R_\ell, M_\ell) \\ &\quad - \frac{\sigma - t_\ell}{t_\ell - t_{\ell-1}} t_{\ell-1}^{\chi-1}\mathcal{K}_i(t_{\ell-1}, S_{\ell-1}, E_{\ell-1}, I_{\ell-1}, A_{\ell-1}, R_{\ell-1}, M_{\ell-1}), \end{aligned} \tag{20}$$

where $i = 1, 2, \ldots, 6$. Thus, (19) and (20) give

$$\begin{cases} S_{\kappa+1}(t) = \bar{S}_0 + \frac{\chi}{\Gamma(\mu)} \sum_{\ell=0}^{\kappa} \int_{t_\ell}^{t_{\ell+1}} (t_{\kappa+1} - \sigma)^{\mu-1} Q_\ell^1(\sigma) d\sigma, \\ E_{\kappa+1}(t) = \bar{E}_0 + \frac{\chi}{\Gamma(\mu)} \sum_{\ell=0}^{\kappa} \int_{t_\ell}^{t_{\ell+1}} (t_{\kappa+1} - \sigma)^{\mu-1} Q_\ell^2(\sigma) d\sigma, \\ I_{\kappa+1}(t) = \bar{I}_0 + \frac{\chi}{\Gamma(\mu)} \sum_{\ell=0}^{\kappa} \int_{t_\ell}^{t_{\ell+1}} (t_{\kappa+1} - \sigma)^{\mu-1} Q_\ell^3(\sigma) d\sigma, \\ A_{\kappa+1}(t) = \bar{A}_0 + \frac{\chi}{\Gamma(\mu)} \sum_{\ell=0}^{\kappa} \int_{t_\ell}^{t_{\ell+1}} (t_{\kappa+1} - \sigma)^{\mu-1} Q_\ell^4(\sigma) d\sigma, \\ R_{\kappa+1}(t) = \bar{R}_0 + \frac{\chi}{\Gamma(\mu)} \sum_{\ell=0}^{\kappa} \int_{t_\ell}^{t_{\ell+1}} (t_{\kappa+1} - \sigma)^{\mu-1} Q_\ell^5(\sigma) d\sigma, \\ M_{\kappa+1}(t) = \bar{M}_0 + \frac{\chi}{\Gamma(\mu)} \sum_{\ell=0}^{\kappa} \int_{t_\ell}^{t_{\ell+1}} (t_{\kappa+1} - \sigma)^{\mu-1} Q_\ell^6(\sigma) d\sigma. \end{cases} \tag{21}$$

After simplifying the integrals in (21), we get the numerical solutions for the COVID-19 epidemic model (3) under the fractal fractional derivative in the Caputo sense with power law as follows:

$$\begin{cases} S_{\kappa+1}(t) = \bar{S}_0 + \frac{\chi\hbar^\mu}{\Gamma(\mu+2)} \sum_{\ell=0}^{\kappa} \Big(t_\ell^{\chi-1}\mathcal{K}_1(t_\ell, S_\ell, E_\ell, I_\ell, A_\ell, R_\ell, M_\ell)\Psi_1(\kappa, \ell) \\ \quad - t_{\ell-1}^{\chi-1}\mathcal{K}_1(t_{\ell-1}, S_{\ell-1}, E_{\ell-1}, I_{\ell-1}, A_{\ell-1}, R_{\ell-1}, M_{\ell-1})\Psi_2(\kappa, \ell) \Big), \\ E_{\kappa+1}(t) = \bar{E}_0 + \frac{\chi\hbar^\mu}{\Gamma(\mu+2)} \sum_{\ell=0}^{\kappa} \Big(t_\ell^{\chi-1}\mathcal{K}_2(t_\ell, S_\ell, E_\ell, I_\ell, A_\ell, R_\ell, M_\ell)\Psi_1(\kappa, \ell) \\ \quad - t_{\ell-1}^{\chi-1}\mathcal{K}_2(t_{\ell-1}, S_{\ell-1}, E_{\ell-1}, I_{\ell-1}, A_{\ell-1}, R_{\ell-1}, M_{\ell-1})\Psi_2(\kappa, \ell) \Big), \\ I_{\kappa+1}(t) = \bar{I}_0 + \frac{\chi\hbar^\mu}{\Gamma(\mu+2)} \sum_{\ell=0}^{\kappa} \Big(t_\ell^{\chi-1}\mathcal{K}_3(t_\ell, S_\ell, E_\ell, I_\ell, A_\ell, R_\ell, M_\ell)\Psi_1(\kappa, \ell) \\ \quad - t_{\ell-1}^{\chi-1}\mathcal{K}_3(t_{\ell-1}, S_{\ell-1}, E_{\ell-1}, I_{\ell-1}, A_{\ell-1}, R_{\ell-1}, M_{\ell-1})\Psi_2(\kappa, \ell) \Big), \\ A_{\kappa+1}(t) = \bar{A}_0 + \frac{\chi\hbar^\mu}{\Gamma(\mu+2)} \sum_{\ell=0}^{\kappa} \Big(t_\ell^{\chi-1}\mathcal{K}_4(t_\ell, S_\ell, E_\ell, I_\ell, A_\ell, R_\ell, M_\ell)\Psi_1(\kappa, \ell) \\ \quad - t_{\ell-1}^{\chi-1}\mathcal{K}_4(t_{\ell-1}, S_{\ell-1}, E_{\ell-1}, I_{\ell-1}, A_{\ell-1}, R_{\ell-1}, M_{\ell-1})\Psi_2(\kappa, \ell) \Big), \\ R_{\kappa+1}(t) = \bar{R}_0 + \frac{\chi\hbar^\mu}{\Gamma(\mu+2)} \sum_{\ell=0}^{\kappa} \Big(t_\ell^{\chi-1}\mathcal{K}_5(t_\ell, S_\ell, E_\ell, I_\ell, A_\ell, R_\ell, M_\ell)\Psi_1(\kappa, \ell) \\ \quad - t_{\ell-1}^{\chi-1}\mathcal{K}_5(t_{\ell-1}, S_{\ell-1}, E_{\ell-1}, I_{\ell-1}, A_{\ell-1}, R_{\ell-1}, M_{\ell-1})\Psi_2(\kappa, \ell) \Big), \\ M_{\kappa+1}(t) = \bar{M}_0 + \frac{\chi\hbar^\mu}{\Gamma(\mu+2)} \sum_{\ell=0}^{\kappa} \Big(t_\ell^{\chi-1}\mathcal{K}_6(t_\ell, S_\ell, E_\ell, I_\ell, A_\ell, R_\ell, M_\ell)\Psi_1(\kappa, \ell) \\ \quad - t_{\ell-1}^{\chi-1}\mathcal{K}_6(t_{\ell-1}, S_{\ell-1}, E_{\ell-1}, I_{\ell-1}, A_{\ell-1}, R_{\ell-1}, M_{\ell-1})\Psi_2(\kappa, \ell) \Big), \end{cases} \tag{22}$$

where

$$\Psi_1(\kappa, \ell) = [(\kappa - \ell + 1)^\mu(\kappa - \ell + \mu + 2) - (\kappa - \ell)^\mu(\kappa - \ell + 2\mu + 2)],$$
$$\Psi_2(\kappa, \ell) = [(\kappa - \ell + 1)^{\mu+1} - (\kappa - \ell)^\mu(\kappa - \ell + \mu + 1)]$$

and $\hbar$ is the step size.

6. Statistical Analysis and Forecasts

This part is dedicated in providing statistical data for the COVID-19 pandemic in Saudi Arabia (see [25]), on it accordingly, we have computed the future predictions of the confirmed cases and deaths by applying the Expert Modeler procedure and SPSS software. A brief discussion of the redobtained outcomes is presented and supported by figures and statistical tables.

6.1. Tables and Figures

Here we present the graphical information about the statistical analysis, given in [25,26] in Figures 1–8. In addition to that we give some test models and statistical predictions are given in Tables 1–5.

Table 1. Summary of the total number of the confirmed cases and deaths in Saudi Arabia.

Months	Confirmed Cases	Deaths	Mean of Confirmed Cases
Mar-20	1563	9	50
Apr-20	19,839	147	4960
May-20	61,982	323	1999
Jun-20	103,052	1119	3435
Jul-20	87,783	1243	2832
Aug-20	40,602	1028	1310
Sep-20	19,366	869	646
Oct-20	12,693	644	409
Nov-20	10,248	501	342
Dec-20	5473	330	177
Jan-21	5212	155	168
Feb-21	9248	116	330
Mar-21	12,361	175	399
Until 22 Apr-21	18,656	195	848
Total	408,078	6854	976

Table 2. Results: model fit statistics and Ljung-Box Q [27].

	Model Fit statistics Ljung-Box Q [27]				
Model	**R-Squared**	**RMSE**	**Statistics**	**DF**	**Sig.**
Death-Model	0.748	1.143	6.951	16	0.974
Confirmed cases Model	0.981	33.954	31.240	18	0.270

Table 3. Test results of the predictive capability of a linear model of confirmed cases in Saudi Arabia.

Dependent Variable: Confirmed Cases **Method: Least Squares** **Sample: 1 March 2020 to 22 April 2021** **Included Observations: 418**				
Variable	**Coefficient**	**Std. Error**	**t-Statistic**	**Prob.**
Predicted	0.990706	0.006538	93.48063	0.0000
R-squared	0.982205			
Adjusted R-squared	0.982163			
Durbin-Watson stat	1.856690			
S.E. of regression	145.3526			
Sum squared resid	878.8992			
F-statistic	22,961.77			
Prob.(F-statistic)	0.000000			

Table 4. Test results of the predictive capability of a linear model of deaths in Saudi Arabia.

Dependent Variable: Deaths **Method: Least Squares** **Sample: 1 March 2020 to 22 April 2021** **Included Observations: 418**				
Variable	**Coefficient**	**Std. Error**	**t-Statistic**	**Prob.**
Predicted	0.983151	0.010517	151.5314	0.0000
R-squared	0.954559			
Adjusted R-squared	0.954449			
Durbin-Watson stat	2.007480			
S.E. of regression	2.929637			
Sum squared resid	3570.433			
F-statistic	8738.629			
Prob.(F-statistic)	0.000000			

Table 5. Expectations of confirmed cases and deaths with their upper and lower limits for COVID-19 in Saudi Arabia for the period from 23 April 2021 to 31 May 2021.

Expectations of Infection Cases				**Expectations of Deaths**			
Date	**LCL Confirmed Cases Model**	**Predicted Confirmed Cases Model**	**UCL Confirmed Cases Model**	**Date**	**LCL Deaths Model**	**Predicted Deaths Model**	**UCL Deaths Model**
23 April 2021	875	1051	1252	23 April 2021	10	12	14
24 April 2021	827	1074	1372	24 April 2021	10	12	15
25 April 2021	796	1098	1479	24 April 2021	10	13	15
26 April 2021	772	1123	1580	26 April 2021	11	13	15
27 April 2021	754	1148	1678	27 April 2021	11	13	16
28 April 2021	739	1173	1774	28 April 2021	11	14	16
29 April 2021	726	1199	1871	29 April 2021	12	14	17
30 April 2021	716	1226	1968	30 April 2021	12	15	17
01 May 2021	707	1253	2066	01 May 2021	12	15	18
02 May 2021	699	1281	2166	02 May 2021	12	15	18
03 May 2021	692	1310	2267	03 May 2021	12	16	19
04 May 2021	686	1339	2370	04 May 2021	12	16	20
05 May 2021	681	1369	2474	05 May 2021	13	16	20
06 May 2021	677	1399	2581	06 May 2021	13	17	21
07 May 2021	673	1431	2690	07 May 2021	13	17	21
08 May 2021	670	1463	2802	08 May 2021	13	17	22
09 May 2021	667	1495	2916	09 May 2021	13	18	23
10 May 2021	665	1528	3033	10 May 2021	13	18	23
11 May 2021	663	1562	3153	11 May 2021	13	19	24
12 May 2021	662	1597	3276	12 May 2021	13	19	25
13 May 2021	660	1633	3402	13 May 2021	13	19	25
14 May 2021	660	1669	3531	14 May 2021	13	20	26
15 May 2021	659	1706	3664	15 May 2021	13	20	27
16 May 2021	659	1744	3799	16 May 2021	13	20	27
17 May 2021	659	1783	3939	17 May 2021	13	21	28
18 May 2021	659	1823	4082	18 May 2021	13	21	29
19 May 2021	659	1864	4229	19 May 2021	13	21	30
20 May 2021	660	1905	4379	20 May 2021	13	22	30
21 May 2021	661	1948	4534	21 May 2021	13	22	31
22 May 2021	662	1991	4693	22 May 2021	13	23	32
23 May 2021	663	2035	4856	23 May 2021	13	23	33
24 May 2021	664	2081	5023	24 May 2021	13	23	33
25 May 2021	666	2127	5195	25 May 2021	13	24	34
26 May 2021	667	2174	5372	26 May 2021	13	24	35
27 May 2021	669	2223	5553	27 May 2021	13	24	36

Table 5. *Cont.*

Expectations of Infection Cases				Expectations of Deaths			
Date	**LCL Confirmed Cases Model**	**Predicted Confirmed Cases Model**	**UCL Confirmed Cases Model**	**Date**	**LCL Deaths Model**	**Predicted Deaths Model**	**UCL Deaths Model**
28 May 2021	671	2272	5739	28 May 2021	13	25	36
29 May 2021	673	2323	5930	29 May 2021	13	25	37
30 May 2021	675	2375	6127	30 May 2021	13	25	38
31 May 2021	678	2428	6328	31 May 2021	13	26	39

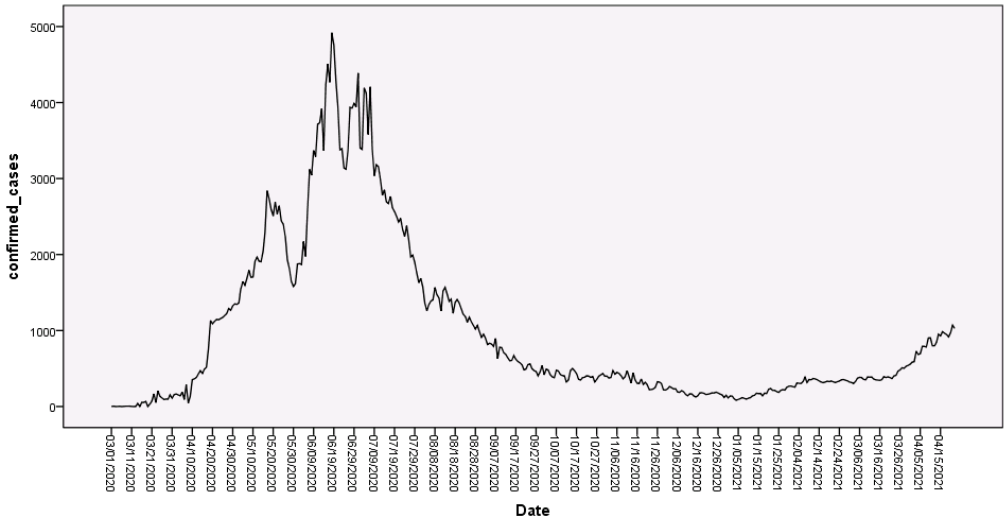

Figure 1. Transmission of confirmed infected cases of COVID-19 in Saudi Arabia for the period from 1 March 2020 to 22 April 2021.

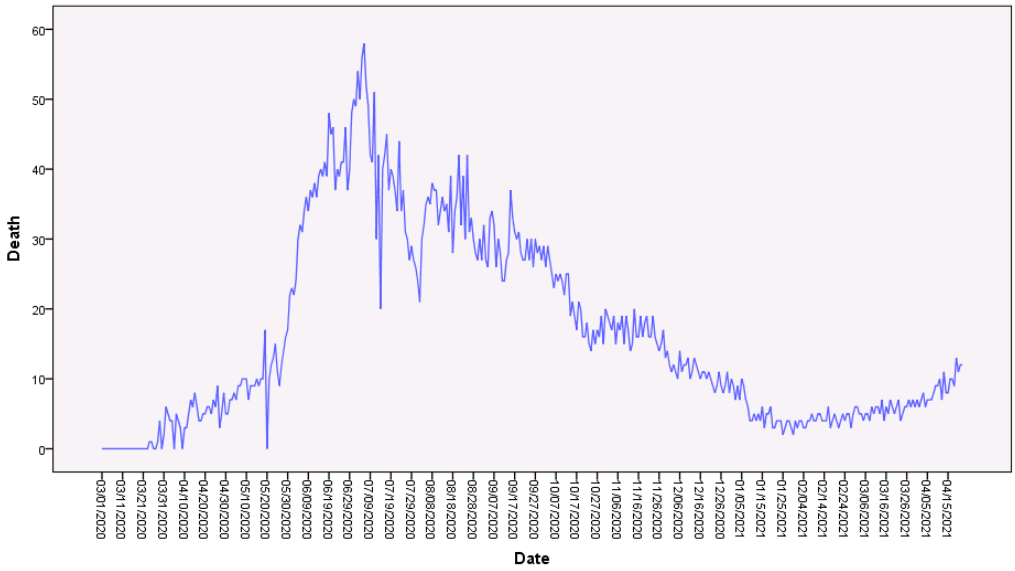

Figure 2. Death cases of COVID-19 in Saudi Arabia for the period from 1 March 2020 to 22 April 2021.

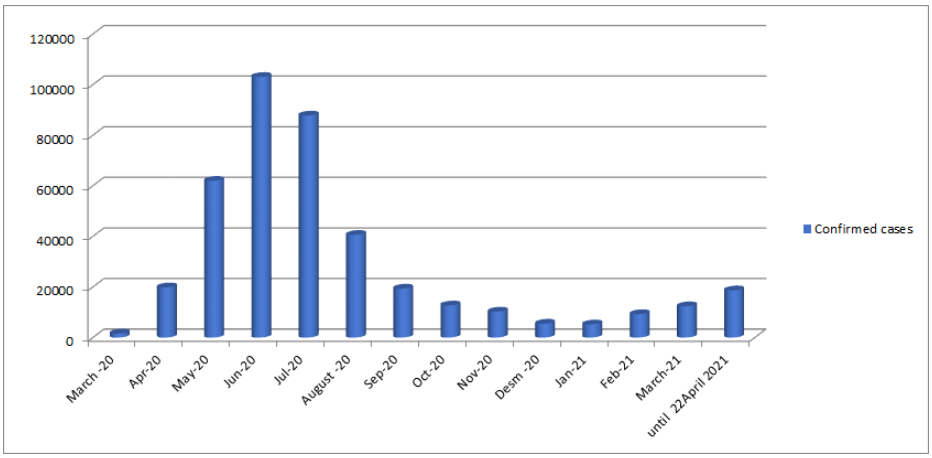

Figure 3. Total confirmed infected cases of COVID-19 in Saudi Arabia for the period from March 2020 to 22 April 2021.

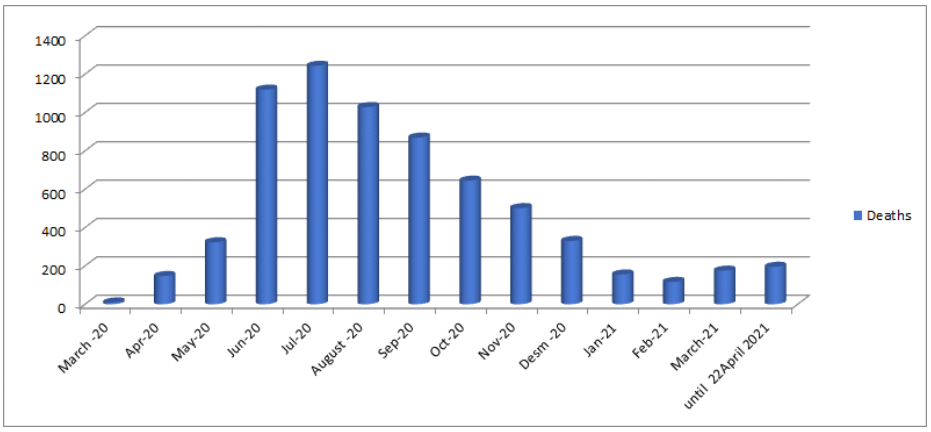

Figure 4. The total number of deaths of COVID-19 in Saudi Arabia for the period from March 2020 to 22 April 2021.

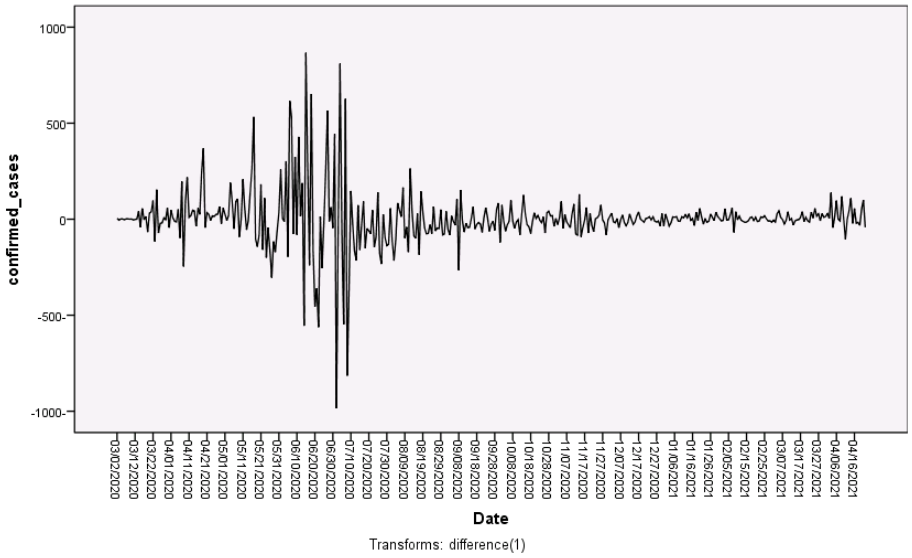

Figure 5. Transmission of the data of confirmed cases of COVID-19 in Saudi Arabia to the first difference.

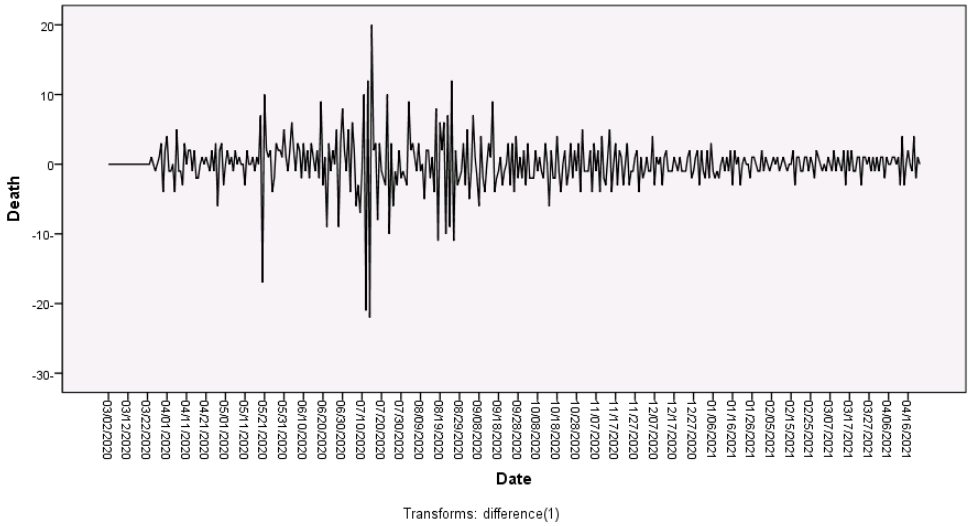

Figure 6. Transmission of the death cases of COVID-19 in Saudi Arabia to the first difference.

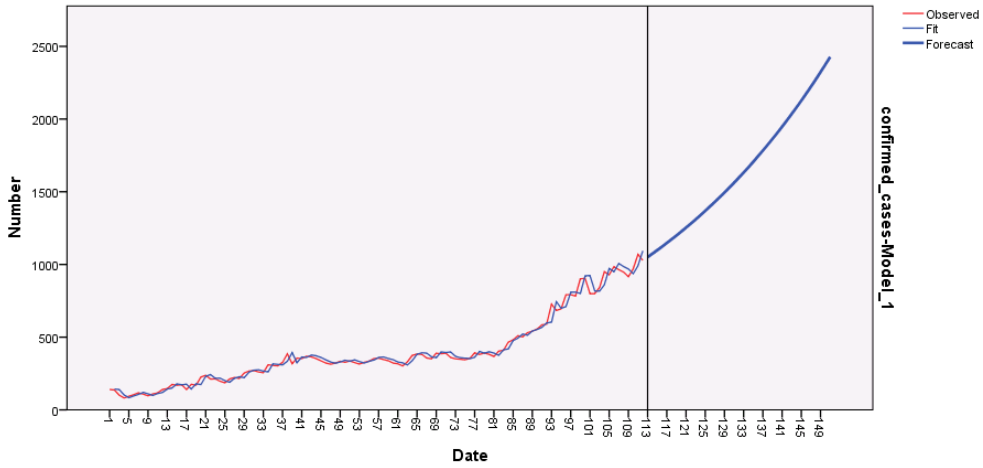

Figure 7. Predicting daily COVID-19 confirmed cases with 95% confidence intervals (CIs) in Saudi Arabia for the period from 23 April 2021 to 31 May 2021.

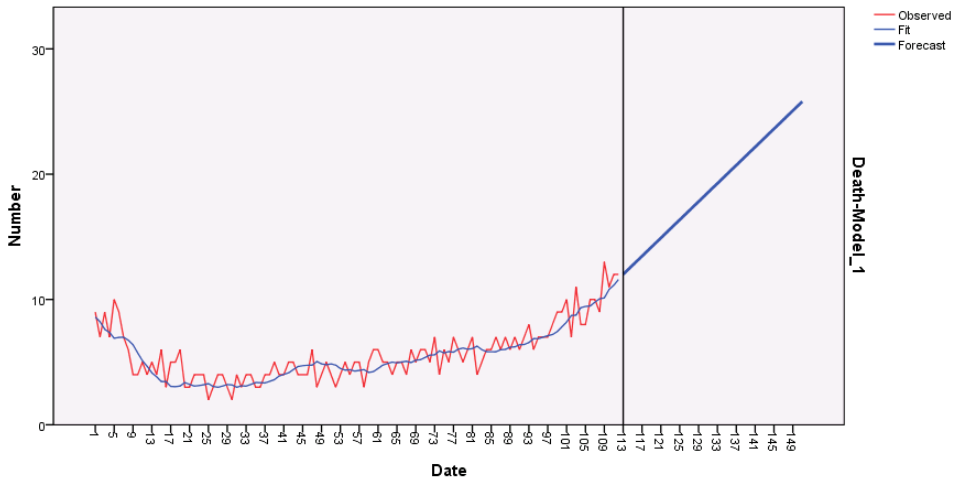

Figure 8. Predicting daily COVID-19 deaths with 95% confidence intervals (CIs) in Saudi Arabia for the period from 23 April 2021 to 31 May 2020.

6.2. Results and Discussion

The most recent statistics about the COVID-19 pandemic and the total number of affirmed cases and deaths in the territory of Saudi Arabia for the period from 1 March 2020 to 22 April 2021 are displayed in Figures 1 and 2. The numbers likewise express that there is a fast and ceaseless expansion in the number of new cases, particularly in the months of May, June, July, and August 2020. The affirmed cases that came to notice during these four months were in excess of 293,419 cases, an average of 0.72 of the all affirmed cases till the end of our study, which added up to 408,078 cases, and there were 3713 deaths—rates of 0.54 from the entire death number. We have seen that it is on the ascent, as the affirmed cases expanded from 1563 in March with an average of 50 cases in a day, then, at that point expanded during April to reach 19,839 with an average of 661 cases. Nonetheless, the number of affirmed cases during May came to 61,982, with an average of 2000 cases. Then, at that point, the quantity of the affirmed cases expanded to reach 103,052 cases toward the end of June with an average of 3435 cases. We additionally saw that during June the cases expanded quickly, which is a much more noteworthy number than the cases during the period 1 March 2020 until 30 May 2020.

We likewise observed that the affirmed cases are persistently diminishing during the period of July to reach 87,783 with an average of 1243, then, at that point, it diminished in August to reach 40,602 with an average 1028 until the end of December 2020 with 5473 cases. In 2021, affirmed recorded cases reached 5212 during the period of January, then, at that point expanded altogether during the long stretches of February and March until reaching 18,656 cases for the 22 days of April.

On the other hand, there has been an increase in the number of deaths from this virus, as nine deaths were recorded for the month of March 2020, then it reached 1243 during the month of July 2020, and then decreased from the months August to December 2020. In 2021, deaths were recorded during January 155, then decreased during February, and then increased during March and April. Table 1 and Figures 3 and 4 illustrate that.

The Expert modeler is an ad-hoc procedure of time series models applied by SPSS for forecasting. It tries to construct a convenient predictive model for one or more series of dependent variables automatically. If there are independent variables regarding the dependent variable, the Expert Modeler Procedure automatically selects only those independent variables that are statistically significant. By default, the Expert Modeler Procedure considers both exponential smoothing and ARIMA models. However, one can limit the Expert Modeler to only search for ARIMA models or to the only search for exponential smoothing models. Furthermore, it is easy to perform and helps in quickly identifying the best models that achieve the required features, making it easier to obtain their forecasts in record time. For more details see [28].

Time series models play a critical role in predicting the actions of phenomena and variables over time and their impact climate science, economics, finance, epidemiology, health engineering, and other different sciences. Many researchers have lately used it to model and forecast future trends in the behavior of many diseases and epidemics. Most of these models include a procedure of four essential steps: initially, identifying the model, secondly, estimating anonymous parameters, thirdly, diagnosis and finally, forecast [29–33]. There are numerous kinds of models for time series that are fitting in predicting, for example, AR, MA, ARMA, ARIMA, ARCH, GARCH. In this manner, the nature and trial of the information for the two series under examination and every one of the hypotheses connected to them (and the consistency of the time series) were confirmed to be utilized in the forecast process. In this regard, there are many transformations that must be used to convert the original data of the non-stationary time series into a stationary time series to be used in the prediction process, such as natural log and differences of the first and second degree. Here, we processed the original data then took the first differences for two series to remove the effect of the general trend, and both series become stable, in order for the model to be valid for predicting deaths and confirmed cases, as in Figures 5 and 6. So they can be utilized in the expectation process. The statistical analysis software (SPSS) version

23 and the Expert Modeler Procedure were utilized to predict new everyday affirmed cases and deaths at a certainty span (95%) for COVID-19 in Saudi Arabia for the period from 22 April 2021 to 31 May 2021 as in Figures 7 and 8 and Table 5.

Table 2 shows the value of the determination coefficient R-squared = 0.748 and 0.981 which are appropriate, which means the model quality used for prediction, and it signifies the data optimally. In addition, there is no problem in the model through the value of the Ljung-Box Q(18) Statistic. A test of the randomness of the residual errors in the model is necessary to be random and must be the level of statistical significance (Sig.) greater than (5%) in order for the data to be distributed randomly. It means that the data follows a random distribution. In this regard, we find the Ljung-Box statistics 6.951 and 31.240 and the statistically significant Sig. = 0.974 and 0.270, which is greater than 0.05; this indicates that the data follows a random distribution.

To examine the predictive capability of the model, the Eviews9 program was used and the least-squares method was applied to estimate a linear model by taking the estimated values of the model as an independent variable and the actual values as a dependent variable. So the closer the estimated parameter is to one, the more the estimated values are close to the actual values. The output of the analysis is observed in Tables 3 and 4 in which the estimated parameters 0.990706 and 0.983151 are close to one. This means the convergence of the estimated values from the actual values, in addition to the model quality in the estimate, and there is a statistically significant $(prob. = 0.000)$ that is less than the approved level of significance, which is statistically significant $(\alpha = 0.05)$.

7. Simulations and Discussion

For the numerical simulations to study the behavior of the susceptible, infectious, treated, and recovered population related to this pandemic that occurred in Saudi Arabia during March 2020 to April 2021, we consider the parameters as in the table below.

Compartments and Parameters	Numerical Values
S_0	34.439456 Millions
E_0	0 Million
I_0	0.408078 Million
A_0	0
R_0	0.406589 Million
M_0	0.09 Million
Λ	$\mu \times N$
μ	1/(76.79 times 365)
υ	0.05
$\bar{\varrho}$	0.02
$\bar{\varpi}$	0.47876
$\bar{\nu}$	0.05
$1/\bar{\nu}$	0.09871
$\bar{\eta}$	0.854302
$\bar{\psi}$	0.000398 $(0 \leq \bar{\psi} \leq 1)$
$\bar{\eta}_\iota$	0.000001231
$\bar{\eta}_\omega$	0.01
ι	0.01

Here some are estimated data and some are fitted with the help of available real data. In addition, the pandemic model is simulated under the fractal fractional order case using a numerical scheme as structured with total population $N = 35.266155$ Million.

In Figure 9, we see that at different fractal fractional order the population of susceptible class is decreasing with a different decay curve. The smaller the values of orders, the faster the decay process and vice versa. In addition, in Figures 10–13, the populations of various compartments are growing. The growth rate is faster at larger values of fractional-fractal

order and vice versa. In Figure 14, we see that the population of numbers of corona virus is also increasing with high speed as infection has increased in the last two months. From these graphical presentations, we conclude that fractal fractional order derivatives explain population dynamics of model of infectious disease more frequently and are easier to understand.

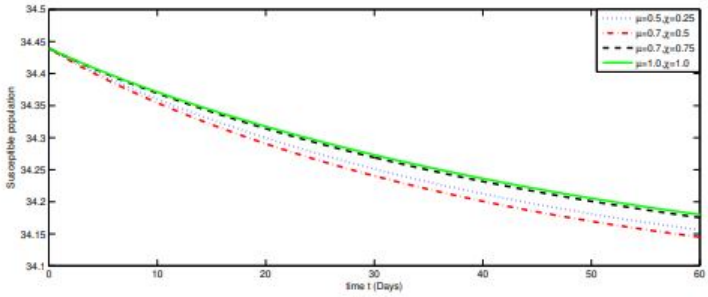

Figure 9. Graphs of numerical solutions at different fractal-fractional order for Susceptible class.

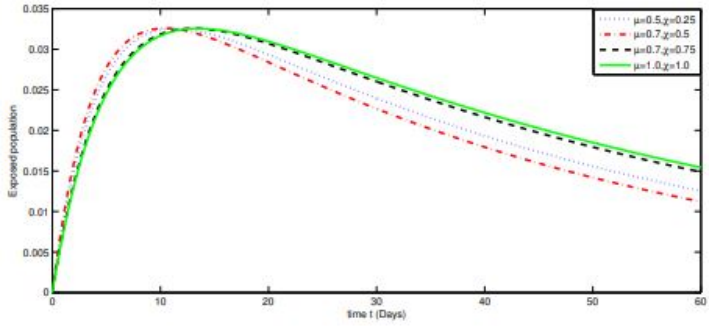

Figure 10. Graphs of numerical solutions at different fractal-fractional order for Exposed class.

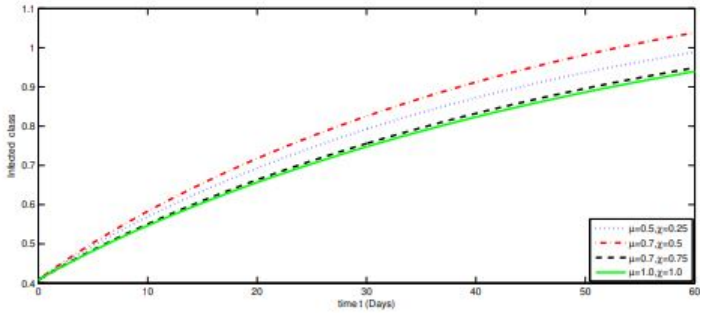

Figure 11. Graphs of numerical solutions at different fractal-fractional order for Infected class.

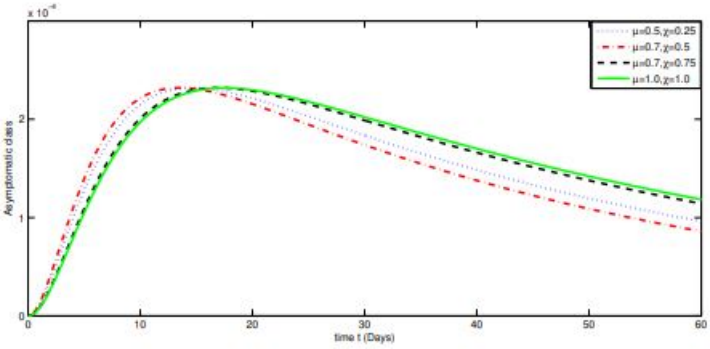

Figure 12. Graphs of numerical solutions at different fractal-fractional order for Asymptomatic class.

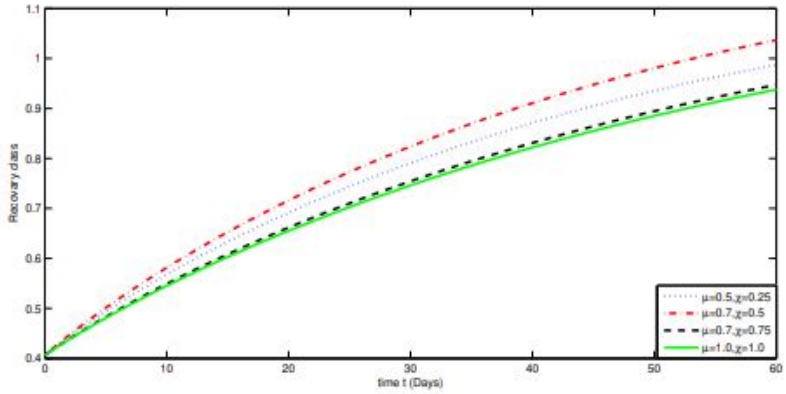

Figure 13. Graphs of numerical solutions at different fractal-fractional order for Recovered class.

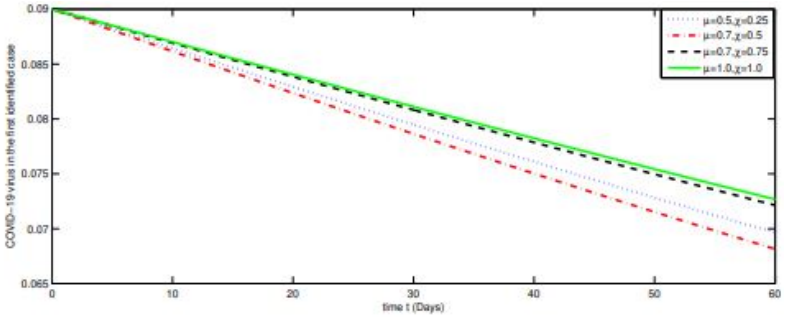

Figure 14. Graphs of numerical solutions at different fractal-fractional order for class *M*.

In Figures 15 and 16, we compare our simulated results in case of infected reported and deaths of KSA as given in Table 5 from 23 April 2021 to 31 May 2021.

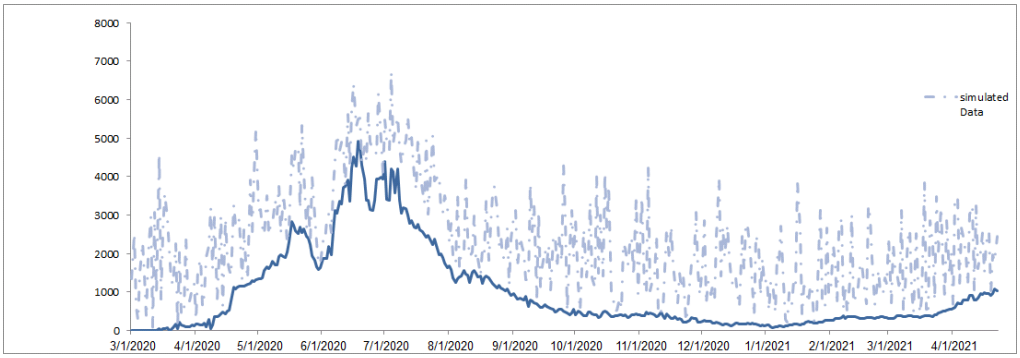

Figure 15. Comparison between real and simulated data for infected class in the considered model.

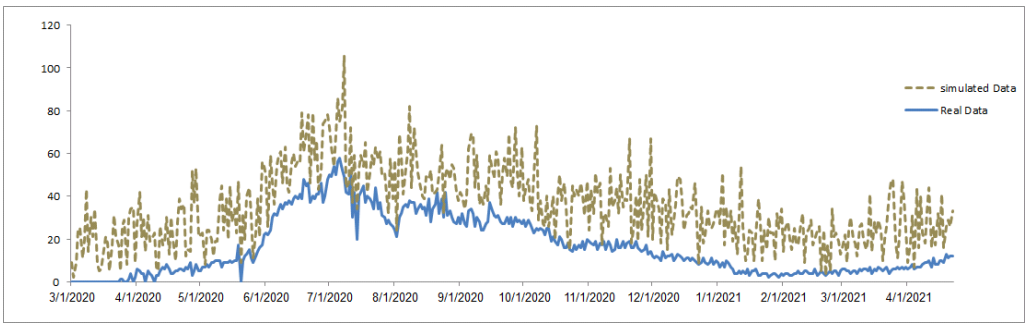

Figure 16. Comparison between real and simulated data for deaths class in the considered model.

8. Conclusions

Using fractal fractional-order derivative, we have successfully established theoretical and computational analysis for a COVID-19 mathematical model. Upon using fixed point approach and Adam–Bashforth method we have achieved the required results. We have presented the numerical results graphically by using various fractional order derivatives and different values of fractal dimension. Some statistical analysis has been provided by taking some real data about Saudi Arabia from 1 March 2020 till 22 April 2021; we have also calculated the fatality rates by using the SPSS, Eviews, and Expert Modeler Procedure, then built forecasts of infection for the period 23 April 2021 to 30 May 2021. The entire investigation of this article revealed that control of the dynamic transmission rate is vital for stopping the transmission of the spreading epidemic.

Author Contributions: Conceptualization, M.B.J., M.S.A. and H.A.W.; methodology, M.B.J., M.S.A. and K.S.; validation, A.S.A. and M.S.A.; formal analysis, M.B.J., M.S.A., K.S. and M.A.A.; investigation, A.S.A. and H.A.W.; writing—original draft preparation, M.B.J., M.S.A. and M.A.A.; writing—reviewand editing, M.S.A. and M.A.A.; supervision, A.S.A. and K.S.; project administration, M.B.J., M.S.A., A.S.A. and H.A.W. All authors have read and agreed to the published version of the manuscript.

Funding: This research was supported by the Deanship of Scientific Research, Imam Mohammad Ibn Saud Islamic University (IMSIU), Saudi Arabia, Grant No. (21-13-18-057).

Institutional Review Board Statement: Not applicable.

Informed Consent Statement: Not applicable.

Data Availability Statement: The data were used to support this study.

Acknowledgments: The authors would like to thank Imam Mohammad Ibn Saud Islamic University for funding this research work. The authors also thank the anonymous reviewers for their valuable remarks on our paper.

Conflicts of Interest: The authors declare that they have no competing interests.

References

1. World Health Organization. Available online: https://www.who.int/emergencies/diseases/novel-coronavirus-2019 (accessed on 11 May 2020).
2. Center for Disease Control and Prevention (CDC). Available online: https://www.cdc.gov/coronavirus/2019-ncov/index.html (accessed on 3 August 2021).
3. Liu, Z.; Magal, Q.; Seydi, O.; Webb, G. A COVID-19 epidemic model with latency period. *Infect. Dis. Model.* **2020**, *5*, 323–337. [CrossRef]
4. Fanelli, D.; Piazza, F. Analysis and forecast of covid-19 spreading in china, italy and france. *Chaos Solitons Fractals* **2020**, *134*, 109761. [CrossRef]
5. Ribeiro, M.H.D.M.; da Silva, R.G.; Mariani, V.C.; dos Coelho, L.S. Short-term forecasting COVID-19 cumulative confirmed cases: Perspectives for Brazil. *Chaos Solitons Fractals* **2020**, *135*, 109853. [CrossRef]
6. Ndairou, F.; Area, I.; Nieto, J.J.; Torres, D.F.M. Mathematical modeling of COVID-19 transmission dynamics with a case study of wuhan. *Chaos Solitons Fractals* **2020**, *135*, 109846. [CrossRef] [PubMed]
7. Ullah, S.; Khan, M.A.; Farooq, M. A fractional model for the dynamics of tb virus. *Chaos Solitons Fractals*. **2018**, *116*, 63–71. [CrossRef]
8. Qureshi, S.; Atangana, A. Mathematical analysis of dengue fever outbreak by novel fractional operators with field data. *Phys. A Stat. Mech. Appl.* **2019**, *526*, 121127. [CrossRef]
9. Khan, M.A.; Azizah, M.; Ullah, S. A fractional model for the dynamics of competition between commercial and rural banks in indonesia. *Chaos Solitons Fractals* **2019**, *122*, 32–46.
10. Podlubny, I. *Fractional Differential Equations*; Elsevier: Amsterdam, The Netherlands, 1998; Volume 198.
11. Kilbas, A.A.; Shrivastava, H.M.; Trujillo, J.J. *Theory and Applications of Fractional Differential Equations*; Elsevier: Amsterdam, The Netherlands, 2006; Volume 204.
12. Caputo, M.; Fabrizio, M. A new definition of fractional derivative without singular kernel. *Progr. Fract. Differ. Appl.* **2015**, *1*, 1–13.
13. Atangana, A.; Baleanu, D. New fractional derivatives with nonlocal and non-singular kernel: Theory and application to heat transfer model. *Therm. Sci.* **2016**, *20*, 763–769. [CrossRef]
14. Khan, M.A.; Atangana, A. Modeling the dynamics of novel coronavirus (2019-ncov) with fractional derivative. *Alex. Eng. J.* **2020**, *59*, 2379–2389. [CrossRef]

15. Abdo, M.S.; Shah, K.; Wahash, H.A.; Panchal, S.K. On a comprehensive model of the novel coronavirus (COVID-19) under Mittag-Leffler derivative. *Chaos Solitons Fractals* **2020**, *135*, 109867. [CrossRef]
16. Thabet, S.T.; Abdo, M.S.; Shah, K. Theoretical and numerical analysis for transmission dynamics of COVID-19 mathematical model involving CaputoFabrizio derivative. *Adv. Differ. Equ.* **2021**, *2021*, 184. [CrossRef] [PubMed]
17. Abdulwasaa, M.A.; Abdo, M.S.; Shah, K.; Nofal, T.A.; Panchal, S.K.; Kawale, S.V.; Abdel-Aty, A.H. Fractal-fractional mathematical modeling and forecasting of new cases and deaths of COVID-19 epidemic outbreaks in India. *Results Phys.* **2021**, *20*, 103702. [CrossRef] [PubMed]
18. Redhwan, S.S.; Abdo, M.S.; Shah, K.; Abdeljawad, T.; Dawood, S.; Abdo, H.A.; Shaikh, S.L. Mathematical modeling for the outbreak of the coronavirus (COVID-19) under fractional nonlocal operator. *Results Phys.* **2020**, *19*, 103610. [CrossRef]
19. Thabet, S.T.M.; Abdo, M.S.; Shah, K.; Abdeljawad, T. Study of transmission dynamics of COVID-19 mathematical model under ABC fractional order derivative. *Results Phys.* **2020**, *19*, 103507. [CrossRef]
20. Almalahi, M.A.; Panchal, S.K.; Shatanawi, W.; Abdo, M.S.; Shah, K.; Abodayeh, K. Analytical study of transmission dynamics of 2019-nCoV pandemic via fractal fractional operator. *Results Phys.* **2021**, *24*, 104045. [CrossRef]
21. Toufik, M.; Atangana, A. New numerical approximation of fractional derivative with non-local and non-singular kernel, application to chaotic models. *Eur. Phys. J. Plus* **2017**, *132*, 444. [CrossRef]
22. Driesschea, P.; Wamough, J. Reproduction numbers and sub-threshold endemic equilibria for compartmental models of disease transmission. *Math. Biosci.* **2002**, *180*, 29–48. [CrossRef]
23. Granas, A.; Dugundji, J. *Fixed Point Theory*; Springer: New York, NY, USA, 2003.
24. Qureshi, S.; Atangana, A. Fractal-fractional differentiation for the modeling and mathematical analysis of nonlinear diarrhea transmission dynamics under the use of real data. *Chaos Solitons Fractals* **2020**, *136*, 109812. [CrossRef]
25. Saudi Arabia: WHO Coronavirus Disease (COVID-19). Available online: https://covid19.who.int (accessed on 22 April 2021).
26. Saudi Arabia COVID-Coronavirus Cases. Available online: https://www.worldometers.info (accessed on 8 August 2021).
27. Ljung, G.M.; Box, G.E.P. On a Measure of a Lack of Fit in Time Series Models. *Biometrika* **1978**, *65*, 297–303. [CrossRef]
28. IBM SPSS Forecasting 22. 2013. Available online: https://www.sussex.ac.uk/its/pdfs/SPSS_Forecasting_22.pdf (accessed on 13 August 2021).
29. Mathevet, T.; Lepiller, M.; Mangin, A. Application of time series analyses to the hydrological functioning of an Alpine karstic system: The case of Bange-L'Eua-Morte'. *Hydrol. Earth Syst. Sci.* **2004**, *8*, 1051–1064. [CrossRef]
30. Khan, F.; Pilz, J. Modelling and sensitivity analysis of river flow in the Upper Indus Basin, Pakistan. *Int. J. Water* **2018**, *12*, 1–21. [CrossRef]
31. Box, G.E.P.; Jenkins, G.M. *Time Series Analysis, Forecasting and Control*; Holden-Day: San Francisco, CA, USA, 1970.
32. Maleki, M.; Mahmoudi, M.R.; Wraith, D.; Pho, K.H. Time series modelling to forecast the confirmed and recovered cases of COVID-19. *Travel Med. Infect. Dis.* **2020**, *37*, 101742. [CrossRef]
33. Yonar, H.; Yonar, A.; Tekindal, M.A.; Tekindal, M. Modeling and forecasting for the number of cases of the COVID-19 pandemic with the curve estimation models, the box-jenkins and exponential smoothing methods. *Eur. J. Med. Oncol.* **2020**, *4*, 160–165. [CrossRef]